energy&fuels

pubs.acs.org/EF
Article

Application of Aqueous Piperazine Solutions for CO_2 Capture in a Waste-to-Energy Plant

Published as part of Energy & Fuels special issue "Recent Advances in Carbon Capture, Utilization, and Sequestration (CCUS)".

Federica Restelli and Stefania Moioli*

Cite This: *Energy Fuels* 2026, 40, 6901−6918

ABSTRACT: The aim of this work is to assess the performance of piperazine-based aqueous solutions for the removal of CO_2 from the flue gas of a waste-to-energy plant, for which no prior studies have been performed. Two solutions are considered, 8 m and 5 m piperazine. The chemical absorption process is simulated in Aspen Plus V.14, and the process configuration is optimized by performing subsequent sensitivity analyses on key design parameters, with the aim of minimizing the reboiler duty required for solvent regeneration. A preliminary economic assessment is also conducted. Comparison of the results indicates that operating with 8 m piperazine is more cost-effective than with 5 m piperazine, with a total annual cost difference of approximately 1.8 M$/y (about 15%). However, from a practical standpoint, a 5 m piperazine solution may be preferred because its larger solid-phase solubility range enables greater process flexibility while avoiding solid precipitation. Given the absence of an upper solubility limit for 5 m PZ (as suggested in the literature), operation at rich loadings above 0.80 mol-CO_2/mol-PZ may be feasible, thereby reducing the thermal energy requirement for solvent regeneration.

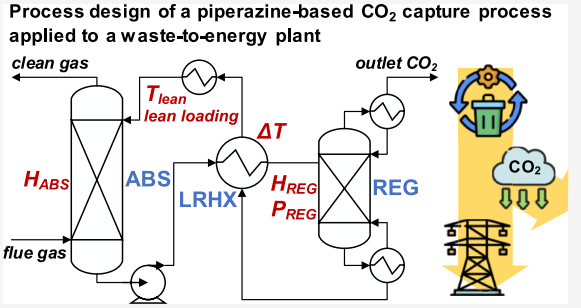

1. INTRODUCTION

In recent years, increasing attention has been devoted to CO_2 emissions from industrial activities, such as coal-fired power plants and steel mills, as these emissions are major contributors to global warming. Consequently, the current research efforts focus on mitigating this type of pollution through the use of biofuels,[1−4] green hydrogen derivatives,[5−9] and the development of increasingly energy-efficient carbon capture technologies.[10−14] These processes enable the removal of a significant portion of CO_2 from the flue gas streams produced by industrial facilities.[15] The captured CO_2 is then prevented from being released into the atmosphere and can instead be stored or reused in applications such as carbonated beverage production or methanol synthesis.

Among the several capture technologies, amine absorption is a well-established technique that has long been employed in natural gas purification, though only a few papers in the literature focus on its application to waste-to-energy plants. For instance, Neerup et al.[16] focused on the analysis of the MEA-based solvent degradation and emissions from a CO_2 capture pilot, Moioli et al. explored the use of MEA for CO_2 capture in a waste-to-energy plant.[17,18] Industrially, only few plants, mainly pilot, are in operation.[15] The process investigated in this work is distinguished by the use of an innovative amine, piperazine (PZ), which has demonstrated several advantages in terms of physicochemical properties compared to more commonly used amines such as monoethanolamine (MEA), diethanolamine (DEA), and triethanolamine (TEA). PZ is a cyclic diamine with two nitrogen atoms at opposite positions, which significantly enhances its reactivity toward CO_2. Numerous studies have investigated the use of piperazine at both laboratory scale[19−21] and pilot scale.[22,23] Experimental investigations by Dugas and Rochelle[19] demonstrated that, at typical absorber operating temperatures (40−60 °C), the liquid-film mass transfer coefficient of PZ-based solutions is more than twice that of MEA at comparable equilibrium CO_2 partial pressures, indicating markedly faster absorption and desorption kinetics and enabling reduced column sizes and lower regeneration energy requirements, with direct benefits in both capital and operating costs. In addition to its favorable kinetics, PZ also exhibits superior CO_2 solubility and capacity, expressed as the difference in the solubility between the lean and rich solution.

Received: November 14, 2025
Revised: March 6, 2026
Accepted: March 11, 2026
Published: March 20, 2026

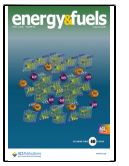

https://doi.org/10.1021/acs.energyfuels.5c05996
Energy Fuels 2026, 40, 6901−6918

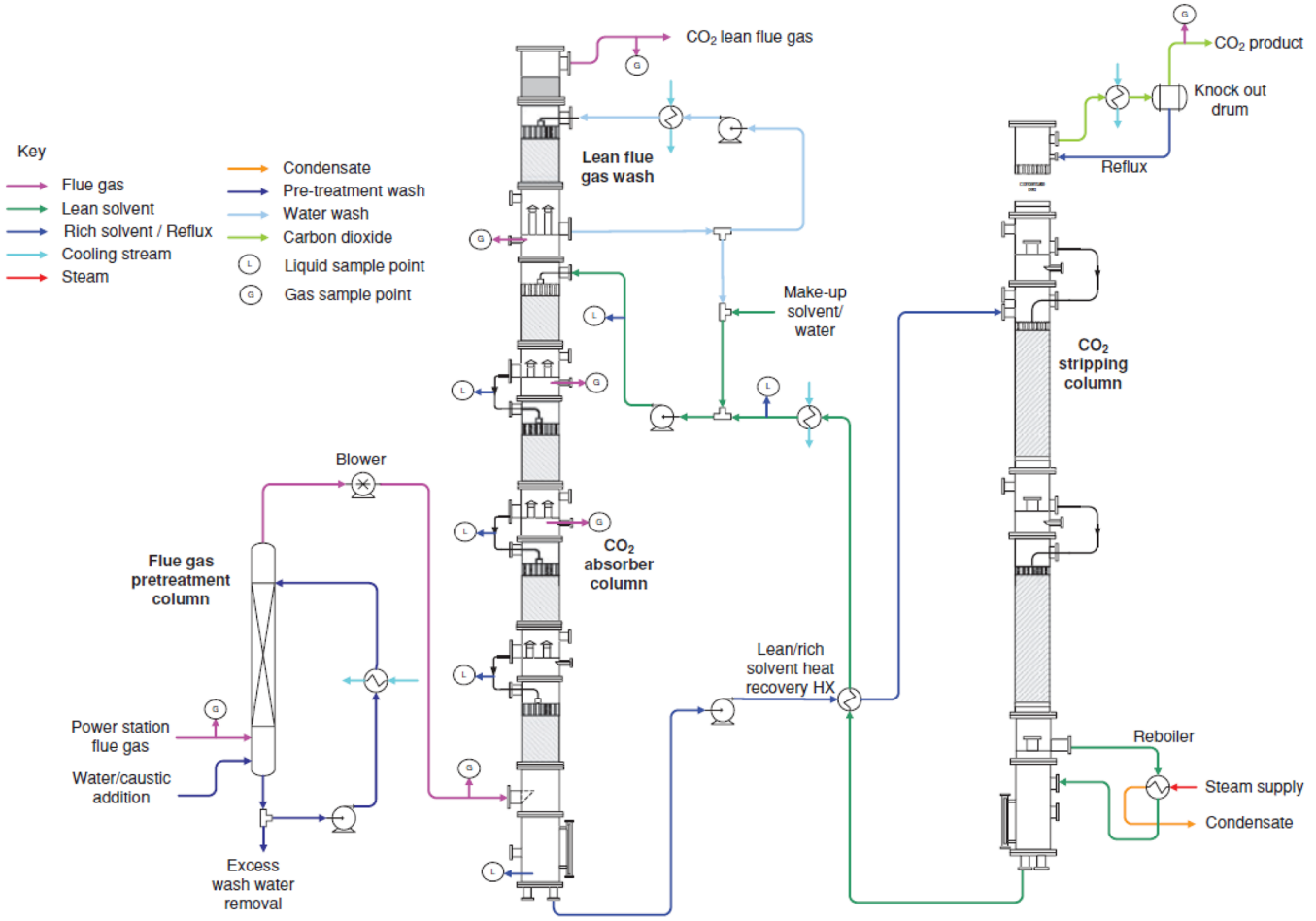

Figure 1. Process flow diagram of the Tarong CO_2 capture pilot plant. Reproduced with permission from ref 22. Copyright 2014 Society of Chemical Industry and John Wiley & Sons, Ltd.

Dugas and Rochelle[19] showed that, at the same CO_2 loading and temperature, PZ solutions sustain significantly higher equilibrium CO_2 partial pressures than MEA, corresponding to greater CO_2 solubilities. Furthermore, CO_2 capacity analyses reveal that an 8 m PZ solution can achieve, on average, approximately 75% higher CO_2 capacity than a 7 m MEA solution under identical operating conditions,[19] attributable to the presence of two amine functionalities in the PZ molecule. Freeman et al.[21] reported the equilibrium CO_2 partial pressure as a function of CO_2 loading for different temperatures (40−100 °C) and PZ concentrations (0.9−8 m PZ), demonstrating that CO_2 solubility in aqueous piperazine solutions exhibits a weak dependence on solvent concentration. Beyond performance, PZ also exhibits enhanced solvent stability, with lower thermal and oxidative degradation rates,[20,24,25] as well as reduced volatility and corrosivity compared to MEA,[20] leading to lower solvent losses, reduced makeup requirements, and improved process economics.[26]

The novelty of this work lies in the design of a PZ-based CO_2 capture plant specifically tailored to treat the flue gas of a waste-to-energy plant. The primary objective is to evaluate the performance of aqueous piperazine solutions at different concentrations. Specifically, an absorption + regeneration process configuration is simulated using Aspen Plus V14,[27] aiming to remove 90% of the CO_2 from a flue gas stream originating from a waste-to-energy plant located in Italy.[17] The simulations are carried out using both 5 m and 8 m aqueous piperazine solutions, selected based on relevant literature data.[19−23,28] The process is optimized in terms of energy consumption by systematically varying key operational parameters one at a time with the goal of minimizing the reboiler heat duty in the regenerator, as it represents the primary contributor to overall process cost. Once the optimal value of each parameter is identified, it is fixed in the simulator prior to performing subsequent sensitivity analysis. A preliminary economic assessment is also performed. Finally, the optimal design choices are discussed in light of the industrial application of the technology.

2. CO_2 CAPTURE WITH AQUEOUS PIPERAZINE SOLUTIONS: LITERATURE REVIEW

The standard configuration of a CO_2 capture process using aqueous amine solutions typically consists of an absorption + regeneration configuration. The main units are an absorption column, where CO_2 is removed from the flue gas by an amine-based solvent; a regeneration column, which is a distillation column or a reboiled stripper, where the absorbed CO_2 is separated from the solvent thanks to the supply of heat, allowing the solvent to be regenerated; and a process−process heat exchanger, where the CO_2-rich solvent leaving the absorber is preheated by exchanging heat with the CO_2-lean solvent from the regenerator before being recirculated to the absorption column. Solvent regeneration is essential, as it would be prohibitively expensive to continuously use fresh solvent for absorption. However, due to solvent losses in the treated gas and

https://doi.org/10.1021/acs.energyfuels.5c05996
Energy Fuels 2026, 40, 6901−6918

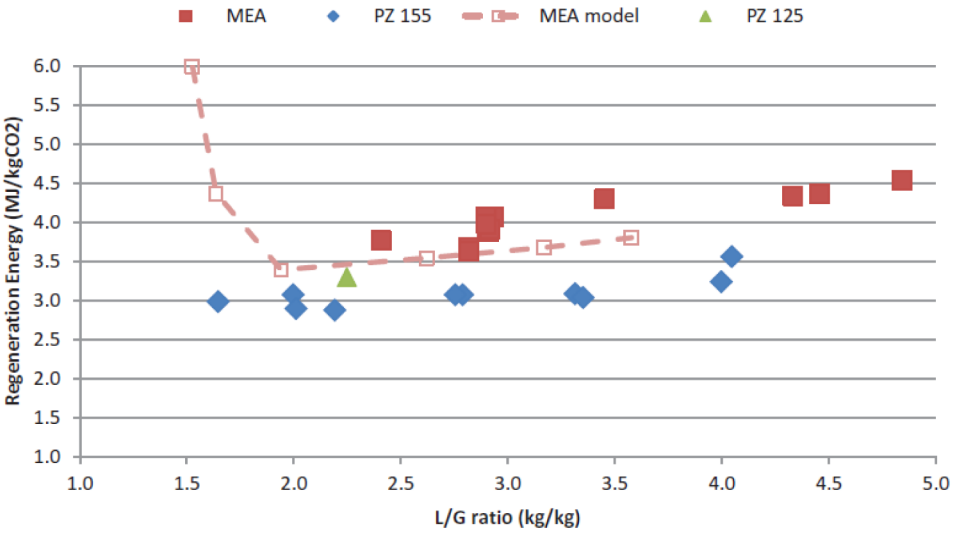

Figure 2. Thermal energy required at the reboiler as a function of the liquid-to-gas ratio. Reproduced with permission from ref 22. Copyright 2014 Society of Chemical Industry and John Wiley & Sons, Ltd.

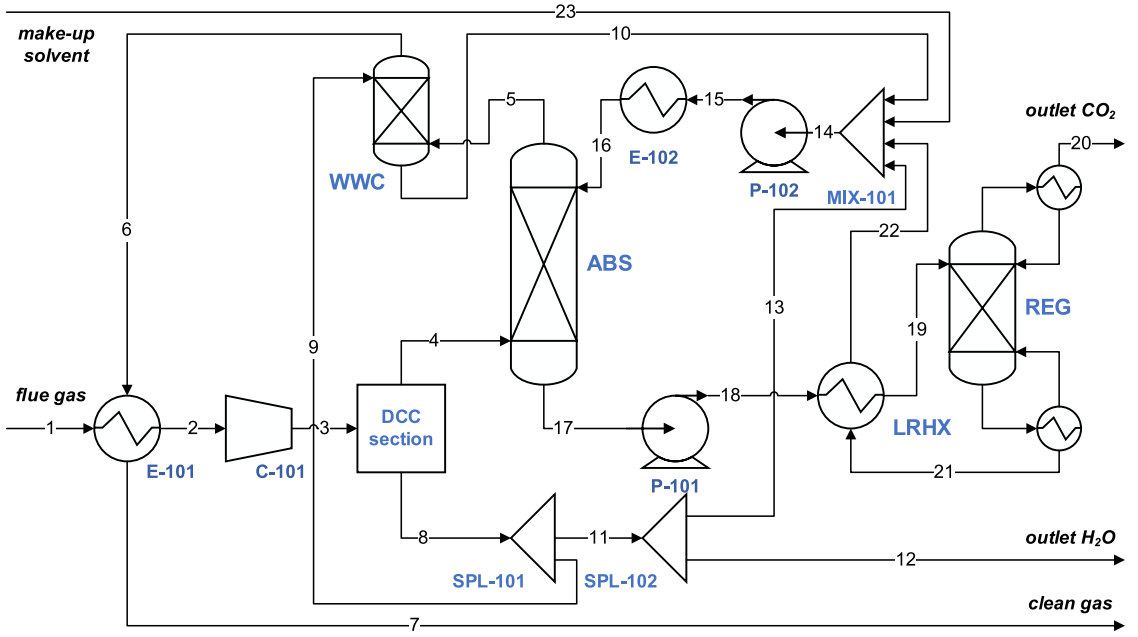

Figure 3. Scheme of the considered CO_2 capture plant.

CO_2 product streams, a makeup solvent flow is required. The primary energy consumption in the process is associated with the reboiler duty required for solvent regeneration.

This standard configuration was studied by Lin et al.[29] for CO_2 capture using 8 m PZ and 9 m MEA solutions. They also proposed alternative configurations for the regeneration section aimed at improving energy performance, albeit at the expense of increased process complexity. Simulations were carried out using Aspen Plus, considering only the regeneration section of the process. The rich loadings for the two amine solutions were 0.40 mol-CO_2/mol-PZ and 0.50 mol-CO_2/mol-MEA, while the lean loadings were varied in the range of 0.30−0.44 mol-CO_2/mol-MEA for the MEA solution and in the range of 0.52−0.68 mol-CO_2/mol-PZ for the PZ solution. The stripper was modeled with a 2 m packing height of Mellapak 250X, and the feed stream consisted of desulfurized flue gas containing 12 mol % CO_2 from coal combustion. The CO_2 capture efficiency was set to 90%. For the base configuration, a reboiler duty of 105.1 kJ/mol-CO_2 is obtained with 8 m PZ, compared to 145.6 kJ/mol-CO_2 with 9 m MEA. These results demonstrate that the use of piperazine reduces the energy consumption associated with solvent regeneration.

Another case study demonstrating the effectiveness of using an aqueous piperazine solution as a solvent for the CO_2 absorption process is the pilot-scale capture plant located in Tarong, Australia. This facility treats a flue gas stream originating from a nearby coal-fired power station. As shown in the pilot plant process scheme (Figure 1), the gas first passes through a pretreatment column ("*Flue gas pretreatment column*" in Figure 1), where it is washed with a dilute caustic solution. It is then directed to the absorption column ("CO_2 *absorber column*" in Figure 1), where most of the incoming CO_2 is removed before

https://doi.org/10.1021/acs.energyfuels.5c05996
Energy Fuels 2026, 40, 6901−6918

Table 1. Characteristics (Molar Vapor Fraction, Pressure, Temperature, Mass Flow Rate, Molar Flow Rate, and Molar Composition) of the Main Streams of the CO_2 Capture Process in the Optimal Scheme Detailed in Section 5.2 for 8 m PZ Case

Stream	1	4	7	16	17	20	21
Molar Vapor Fraction	1	1	1	0	0	1	0
Pressure [bar]	0.98	1.35	1.30	1.40	1.35	4.00	4.02
Temperature [°C]	128.3	35.0	108.3	40.0	39.3	30.0	145.0
Mass Flow Rate [kg/h]	62913	57439	55732	65920	67594	6578	61016
Molar Flow Rate [kmol/h]	2260.4	1956.6	2076.5	2337.2	2069.3	150.4	2067.7
Molar Composition [%]							
PZ	0.0000	0.0000	0.0001	12.1528	12.7608	0.0000	13.6526
H_2O	17.0885	4.2155	16.9139	84.3229	77.0826	1.0920	82.3934
CO_2	7.3014	8.4343	0.7824	3.5243	10.1552	98.8869	3.9540
N_2	66.5721	76.9089	72.4657	0.0000	0.0011	0.0167	0.0000
O_2	9.0380	10.4414	9.8380	0.0000	0.0003	0.0043	0.0000

being vented through the power station exhaust duct. The solvent is subsequently regenerated in a distillation column equipped with a partial reboiler and a partial condenser ("*CO_2 stripping column*" in Figure 1), and then recycled to the absorber.

Several experimental campaigns were conducted at this pilot plant by varying the selected operating parameters. The first campaign employed a 7 m MEA solution (approximately 30 wt %) as the solvent,[30] followed by a second campaign using an 8 m PZ solution.[22] In both the cases, the flue gas originated from the same coal-fired power station and the column configurations remained identical. The flue gas flow rate was approximately 500 kg/h, and the bottom temperature of the regenerator ranged between 115 and 120 °C. The average regeneration pressure was around 180−190 kPa, and the CO_2 capture efficiency averaged about 80%, reaching a peak of 93%. Cousins et al.[22] analyzed the variation of the energy required for solvent regeneration as a function of the liquid-to-gas ratio (L/G) in the absorber. Figure 2 shows the values of regeneration energy as a function of L/G obtained in the two campaigns. Theoretically, this curve should exhibit a minimum: at high liquid flow rates, the sensible heat required to heat the solvent dominates, whereas at low flow rates, the heat needed for vapor generation becomes predominant. However, no such minimum was observed, as operation at very low liquid flow rates proved problematic, and the corresponding results were, therefore, not reported.[22] Nevertheless, the results clearly show that the regeneration energy required when using the 8 m PZ solution is lower than that for the 7 m MEA solution across all tested L/G values, demonstrating the superior performance of the 8 m PZ solvent.

3. PROCESS SCHEME OF THE CONSIDERED CO_2 CAPTURE PLANT

The aim of the CO_2 capture process is to absorb 90% of the CO_2 initially present in the flue gas from a waste-to-energy plant (the target value of 90% is chosen based on values commonly adopted in previous studies from the literature[17,29,31]). The CO_2 capture plant employs an aqueous piperazine (PZ) solution and is located downstream of existing treatment units that reduce SO_x, NO_x and particulate matter to comply with national regulations. The flue gas considered is identical to that used by Moioli et al.[17] in their study of a waste-to-energy plant, where a full-scale CO_2 capture plant based on absorption with an aqueous MEA solution was designed. The flue gas (stream 1 in Figure 3 and Table 1) is characterized by a total mass flow rate of 62913 kg/h, a pressure of 0.98 bar, and a temperature of 128.3 °C. Its molar composition is 17.0885% H_2O, 7.3014% CO_2, 66.5721% N_2 and 9.0380% O_2. The concentrations of NO_x, SO_x, and aerosols in the flue gas are assumed to be negligible, considering that the CO_2 capture unit is located downstream of the conventional emission abatement systems typically installed in a waste-to-energy plant.[17]

Figure 3 shows the proposed process configuration. The absorption column (ABS), the regeneration column (REG), and the lean-rich heat exchanger (LRHX) represent the core of the process. The pressure of the rich solvent (stream 17) leaving the absorber is increased by pump P-101 before entering LRHX, since the regeneration section operates at a higher pressure than the absorption section. A water-wash section is also included downstream of the absorber. Its purpose is to recover, through the use of a wash water stream (stream 9), any piperazine present in the flue gas leaving the absorber (stream 5), thereby ensuring compliance with the emission limits for this amine set by government regulations. The stream leaving the water-wash column (WWC) (stream 10) is then recycled to mixer MIX-101 to reduce the required piperazine makeup flow rate. Upstream of the absorber, there is a flue gas pretreatment section consisting of a process−process heat exchanger (E-101), a blower (C-101), and a direct contact cooler (DCC section). The purpose of this section is to cool the incoming flue gas stream, increase its pressure to promote water vapor condensation, and reduce the water content. These operations help improve the performance of the absorption column. The flue gas, entering the process at 128.3 °C, is precooled in E-101 through heat exchange with the clean gas leaving the WWC.[17] The clean gas must be reheated before discharge to the stack of the waste-to-energy plant, where a minimum temperature of 100 °C is required. Since E-101 is a gas−gas heat exchanger, its effectiveness is expected to be relatively low; hence, a minimum temperature approach of 20 °C is assumed. The purpose of C-101 is to compensate for the pressure drops in the downstream processing units, ensuring that the treated gas can be released to the atmosphere at atmospheric pressure. The DCC section (represented as a box in Figure 3) consists of a column with a few equilibrium stages, where cold water flows countercurrently to the flue gas, promoting condensation of the water vapor contained in the gas stream. The unit also includes a water recirculation system composed of a cooler, a pump, and a splitter. A detailed description of this section, along with its corresponding process flow diagram, can be found in the work by Moioli et al.[17] The water separated in the DCC section can then be partially reused for the washing operation (stream 9) and partially recycled to mixer MIX-101 (stream 13), thereby reducing the required water makeup. As in all absorption + regeneration processes, it is necessary to add a solvent makeup stream (stream 23) to

https://doi.org/10.1021/acs.energyfuels.5c05996
Energy Fuels 2026, 40, 6901−6918

compensate for the piperazine lost in the product streams and maintain the overall mass balance of the system. Minimization of the solvent makeup flow rate leads to a reduction in operating costs. By mixing the solvent makeup stream with the water streams from WWC and DCC section and the regenerated solvent (stream 22), after cooling in LRHX, the lean solvent stream is obtained. Before being fed to ABS, the lean solvent is pumped in P-102 and cooled in E-102.

4. METHODOLOGY

4.1. Process Design of the CO_2 Capture Plant

The simulation of the CO_2 capture process is carried out considering the removal of 90% of the CO_2 initially present in the flue gas by absorption with an aqueous piperazine solution. This capture efficiency is obtained by adjusting the solvent flow rate to the absorption column. Two PZ concentrations are considered, 5 m and 8 m. The process is optimized to minimize thermal power consumption at the reboiler of the regenerator. The aim is to determine the optimal values of the main design variables of the process. Once the plant is constructed, the implemented control strategy will ensure that operating conditions are maintained at the identified design optimum.

The scheme is optimized by choosing the lean loading (the ratio in the liquid phase between the moles of CO_2, including both the unreacted and the reacted CO_2, and the moles of PZ, including both the unreacted and the reacted PZ), the absorber packing height, the regeneration column packing height, the regeneration column pressure, the temperature of the lean solvent, and the approach temperature difference in the lean/rich heat exchanger.

When performing a sensitivity analysis to evaluate the effect of a given parameter, all the other parameters are kept at the same values to avoid the overlapping of several effects due to the variation of multiple parameters at the same time.

All of the analyses are carried out in Aspen Plus V14[27] by performing rate-based simulations for the columns. For the thermodynamic description of the system, the unsymmetric electrolyte NRTL model[32−34] is used for the liquid phase, and the PC-SAFT Equation of State[35−37] is adopted for the vapor phase. The set of reactions reported below is used to model the reacting system within the columns present in the simulation.

$$2H_2O \leftrightarrow H_3O^+ + OH^- \quad (1)$$

$$HCO_3^- + H_2O \leftrightarrow CO_3^{2-} + H_3O^+ \quad (2)$$

$$(PZ)H^+ + H_2O \leftrightarrow PZ + H_3O^+ \quad (3)$$

$$H(PZ)COO + H_2O \leftrightarrow (PZ)COO^- + H_3O^+ \quad (4)$$

$$CO_2 + OH^- \rightarrow HCO_3^- \quad (5)$$

$$HCO_3^- \rightarrow CO_2 + OH^- \quad (6)$$

$$PZ + CO_2 + H_2O \rightarrow (PZ)COO^- + H_3O^+ \quad (7)$$

$$(PZ)COO^- + H_3O^+ \rightarrow PZ + CO_2 + H_2O \quad (8)$$

$$(PZ)COO^- + CO_2 + H_2O \rightarrow (PZ)COO^{2-} + H_3O^+ \quad (9)$$

$$(PZ)COO^{2-} + H_3O^+ \rightarrow (PZ)COO^- + CO_2 + H_2O \quad (10)$$

The rate constants for reactions 5−10 are calculated using an Arrhenius-type expression (eq 11). The pre-exponential factor (k) and the activation energy (E_a) are listed in Table 2.

$$\text{Rate constant} = k \times \exp\left(-\frac{E_a}{RT}\right) \quad (11)$$

Table 2. Pre-exponential Factor (k), the Activation Energy (E_a), and Concentration Basis of the Arrhenius-Type Expression for Calculating the Reaction Rate Constants for Reactions (5)−(10), Derived from the Work of Pinsent et al.[38] and Bishnoi and Rochelle[39,40]

Reaction	k	E_a [MBtu/lbmol]	Concentration basis
(5)	1.33×10^{17}	23.8482	mole gamma
(6)	6.63×10^{16}	46.18	mole gamma
(7)	1.70×10^{10}	0.5742	mole gamma
(8)	3.40×10^{23}	25.488	mole gamma
(9)	1.04×10^{14}	156470.469	mole gamma
(10)	3.20×10^{20}	15.6456	mole gamma

The absorber, regenerator, and water-wash column are all packed columns simulated using the rate-based approach. The main features of these columns are reported in Table 3.

Table 3. Main Features of the Absorber, Regenerator, and Water-Wash Column

Column	ABS	REG	WWC
Operating pressure [bar]	1.32	design variable	1.3
Column pressure drop [bar]	0.03	0.02	0
Condenser	none	partial vapor	none
Reboiler	none	kettle	none
Packing type	Mellapak 250X	Mellapak 250X	Mellapak 250X
Column diameter [m]	2.4	1.0−1.3	2
Packing height [m]	design variable	design variable	4
Number of stages of packing height discretization	40	20	10

The column diameter must, in principle, be adjusted in each simulation to ensure that the hydraulic profile remains within the operational limits along the column. The column diameters reported in Table 3 provide an approach to flooding of approximately 80%. The use of a smaller column diameter for the WWC is common practice in industrial applications.[17] The packing height is a design variable for both ABS and REG, while the operating pressure is a design variable only for REG. Pressure drops of 0.03 and 0.02 bar are considered for the absorption and regeneration columns, respectively, whereas the pressure drop in the water-wash column is assumed negligible, considering its low height. The packing height is discretized in the simulation using 40 stages for the absorber and 10 stages for both the regeneration and the water-wash column. Rate-based calculations are performed for all of the columns. For each stage, the liquid phase is assumed to be perfectly mixed. Therefore, its bulk properties correspond to the outlet conditions of the liquid stream leaving the stage. The vapor phase is assumed to follow plug-flow behavior, and its bulk properties are calculated as the average of the inlet and outlet vapor conditions. Film resistances are modeled by considering diffusion resistance without

https://doi.org/10.1021/acs.energyfuels.5c05996
Energy Fuels 2026, 40, 6901−6918

chemical reactions in the vapor film and diffusion resistance with chemical reactions in the liquid film. The mass transfer coefficients and interfacial area are estimated using the correlation proposed by Bravo et al.,[41] and the heat transfer coefficient is calculated using the Chilton−Colburn analogy.[42]

ABS and WWC are absorption columns; hence, a single specification, namely the packing height, is sufficient to fully constrain the problem. In contrast, REG is a distillation column equipped with a partial reboiler (kettle type) and a partial condenser. Consequently, in addition to the packing height, two further specifications are required to solve this column, one related to the temperature of the vapor product (stream 20) and another to the amount of CO_2 removed from the rich solvent, which must match the amount removed in the absorption and water-wash sections. To satisfy these specifications, two operating variables are adjusted, the reflux ratio and the bottoms-to-feed ratio.

4.2. Cost Estimation

The type of economic analysis performed is a *Preliminary Design Estimate*.[43] Only the pieces of equipment expected to represent the highest costs for each unit are considered (columns, heat exchangers, pumps and compressors). In the present simulation, these are the absorber (ABS), the regenerator (REG), the water-wash column (WWC), the direct contact cooler (DCC section), the gas−gas heat exchanger (E-101), the water-cooled heat exchanger (E-102), the liquid−liquid heat exchanger (LRHX), the condenser and reboiler of REG, the pumps (P-101, P-102) and the compressor (C-101). For the reboiler, a U-tube bundle heat exchanger is assumed and the condenser is assumed to be of the floating-head type. All other heat exchangers are plate-type and operate in counter-current flow. Both the pumps and compressors are assumed to be centrifugal. All equipment and components are made of stainless steel.

The investment costs are calculated according to the methodology described by Turton et al.,[43] which has an accuracy of 10−40% in line with the *preliminary design estimate* (Class 3 estimate, according to AACE International Recommended Practice No. 17R-97[44]), and are briefly summarized in the following.

First, the purchased base cost $\left(C_p^0\right)$ of the equipment, made with a base material (carbon steel) and operating under ambient pressure conditions, is calculated according to eq 12:

$$\log_{10}(C_p^0) = K_1 + K_2 \log_{10}(A) + K_3[\log_{10}(A)]^2 \quad (12)$$

The parameter A represents the characteristic size of the considered unit. The coefficients K_1, K_2, and K_3 depend on the type of unit and on the reference year. The values of these constants are reported by Turton et al.[43] referring to the year 2001. The value of C_p^0 calculated using eq 12 must be updated to the reference year for the present economic evaluation (January 2025) using the Chemical Engineering Plant Cost Index (CEPCI), as in eq 13:

$$C_p^0 = C_{p,ref}^0 \left(\frac{\text{CEPCI}_{01\text{-}2025}}{\text{CEPCI}_{ref}} \right) \quad (13)$$

The bare module cost (C_{BM}) of the equipment, calculated as in eq 14, accounts for the deviations of C_p^0 from the standard conditions through multiplication factors that take into account the type of unit, its pressure (F_p), and the material of construction (F_{BM}).

$$C_{BM} = C_p^0 F_{BM} = C_p^0 (B_1 + B_2 F_p F_M) \quad (14)$$

The coefficients B_1 and B_2 are constants that depend on the type of unit and account for direct and indirect additional costs. Their values are reported by Turton et al.[43]

The total C_{BM} is calculated by summing the C_{BM} values of all units. A spare pump is included for both P-101 and P-102. The total module cost (C_{TM}) is then obtained by multiplying the total C_{BM} by 1.18 to account for the contingency. Based on this cost, the grassroots cost (C_{GR}) is determined using eq 15, where C_{BM}^0 represents the bare module cost under base conditions, with both F_p and F_M set to 1 for each piece of equipment.

$$C_{GR} = C_{TM} + 0.50 \sum_i C_{BM,i}^0 \quad (15)$$

Finally, the capital expenditure ($CapEx$) is obtained by adding the initial solvent cost to the C_{GR}. The prices of piperazine and water are assumed to be 35.7 \$/kg[45] and 0.0018 \$/kg,[46] respectively.

The operating expenditure ($OpEx$) is estimated assuming that the plant operates for 7900 h per year. The $OpEx$ accounts for various contributions, which can be categorized into direct manufacturing costs, fixed manufacturing costs, and general manufacturing expenses, as reported in Table 4.

Table 4. Operating Expenditure Estimation[43]

Cost item	Value
Direct manufacturing costs	
raw material	C_{RM}
utilities	C_{UT}
operating labor	C_{OL}
direct supervisory and clerical labor	$0.18 \times C_{OL}$
maintenance and repair	$0.07 \times CapEx$
operating supplies	$0.009 \times CapEx$
laboratory charges	$0.15 \times C_{OL}$
patents and royalties	$0.03 \times OpEx$
Fixed manufacturing costs	
local taxes and insurance	$0.04 \times CapEx$
plant overhead costs	$0.708 \times C_{OL} + 0.036 \times CapEx$
General manufacturing expenses	
administration costs	$0.177 \times C_{OL} + 0.009 \times CapEx$
distribution and selling costs	$0.1 \times OpEx$
research and development	$0.05 \times OpEx$
contingency	$0.05 \times OpEx$

The only raw material considered in this study is the solvent makeup. In principle, PZ makeup should also account for losses due to solvent degradation. However, since PZ degrades much more slowly than MEA, this contribution is neglected. Therefore, the PZ makeup considered here includes only amine losses due to volatility, as calculated by the simulator. Regarding utilities, cooling water is assumed as the cooling medium in heat exchanger E-102, in the DCC section, and in the condenser of REG, at a cost of 0.441 \$/GJ. Low-pressure steam (5 barg, 160 °C) is used to supply the heat required by the reboiler of REG at a cost of 7.71 \$/GJ. Electricity is used to power the compressor C-101 and the pumps P-101 and P-102, at a cost of 23.1 \$/GJ. The utility costs are estimated using the CAPCOST program,[43] with input data based on the average industrial prices of natural gas[47] and electricity[48] in the United States for January 2025, as reported by the U.S. Energy Information Administration (EIA).

https://doi.org/10.1021/acs.energyfuels.5c05996
Energy Fuels 2026, 40, 6901−6918

The cost of labor is calculated by determining the number of operators per shift (N_{OL}) as a function of P (number of solid-handling units) and N_{np} (number of fluid-handling units), as reported in eq 16:

$$N_{OL} = (6.29 + 31.7 \times P^2 + 0.23 \times N_{np})^{0.5} \quad (16)$$

For the studied process configuration, $P = 0$ and $N_{np} = 8$. Pumps are excluded from the N_{np} calculation, as stated by Turton et al.[43] An average annual operator wage of $45000/year is assumed.

Finally, the total operating expenditure ($OpEx$) is obtained by summing all of the items listed in Table 4. Knowing both the capital cost ($CapEx$) and the operating cost ($OpEx$), the total annual cost is calculated as the sum of the annualized investment cost, computed as $CapEx$ divided by the plant lifetime (assumed to be 25 years), and the $OpEx$.

5. RESULTS AND DISCUSSION

5.1. Process Design of the CO_2 Capture Plant

In this section, the sensitivity analyses are carried out by varying certain operating variables of the process. The parameters considered in the study are the same for both the simulations performed with 8 m PZ and those with 5 m PZ. In particular, as previously stated, the optimum for each process variable of interest is assessed in relation to the reboiler heat duty of the regenerator. For each sensitivity analysis, the optimum value of the variable under investigation is identified and then kept constant in the subsequent analyses. The study began by examining the effect on the reboiler duty of the lean loading (mol-CO_2/mol-PZ in the lean solvent stream entering the absorption column) and the absorber height (H_{ABS}). Subsequently, the effect on the reboiler duty of the following variables is evaluated in sequence: regenerator height (H_{REG}), regenerator pressure (P_{REG}), and lean solvent temperature (T_{lean}). Finally, by varying the approach temperature difference (ΔT) in the lean-rich heat exchanger, a preliminary economic analysis is performed considering both operating and capital costs. The initial values for the optimization variables are set equal to 0.30 for lean loading, 16 m for H_{ABS}, 10 m for H_{REG}, 4 bar for P_{REG}, 35 °C for T_{lean}, and 20 °C for ΔT. These values are kept constant during the initial sensitivity analyses to ensure consistency across cases. They are subsequently updated as the optimization proceeds.

5.1.1. Choice of the Absorber Packing Height and the Lean Loading. The first step involves defining the range of lean loadings to be simulated. When this range is selected, it is essential to remain within the solid-phase solubility limits of the solvent, as illustrated in Figure 4. Indeed, it is crucial to avoid the formation of solid precipitates, which would otherwise reduce the amount of amine effectively active in the process. In Figure 4, the CO_2 loading indicates the concentration of CO_2 in solution, expressed as moles of CO_2 per mole of alkalinity (or per mole of N), which corresponds to two moles of CO_2 per mole of PZ (since piperazine contains two N atoms). The two solubility curves illustrate how the transition temperature varies with the CO_2 loading. On the left-hand side of the graph, for CO_2-lean solutions, the solid precipitate is PZ·6H_2O. On the right-hand side, for CO_2-rich solutions, there is another precipitation curve present only for 8 m PZ, beyond which the formation of another solid precipitate (H^+PZCOO^-·6H_2O) occurs. Cousins et al.[22] reported that at typical operating temperatures of 40−150 °C, the CO_2 loading for an 8 m PZ solution should be maintained in the range of 0.20−0.80 mol-CO_2/mol-PZ. For 5 m PZ, as reported by Chen et al.,[28] the upper solid solubility limit is absent.

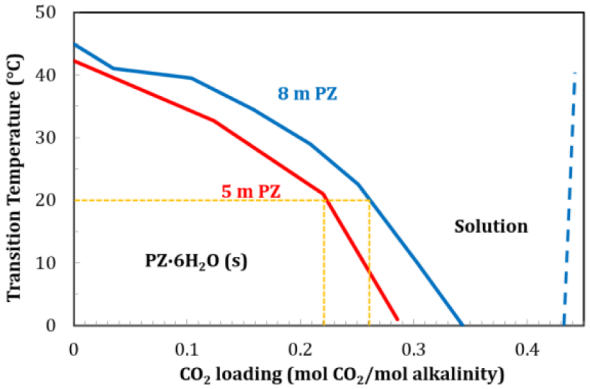

Figure 4. Comparison of 5 and 8 m PZ solid solubility. Reproduced with permission from ref 28. Copyright 2017 Elsevier.

According to the literature, lean loading is typically between 0.30 mol-CO_2/mol-PZ and 0.60 mol-CO_2/mol-PZ.[28,29,49] In this work, the analyzed range is 0.20−0.40 mol-CO_2/mol-PZ (corresponding to 0.10−0.20 mol-CO_2/mol-alkalinity), with increments of 0.02 mol-CO_2/mol-PZ. As shown in Figure 4, at temperatures of 35−40 °C, which correspond to the lowest temperatures in the process for streams containing CO_2 and PZ (specifically, the lean solvent entering the absorption column, stream 16 in Figure 3), this range falls within the region without solid precipitation. Regarding precipitation due to excessive CO_2 loading, attention must also be paid to the composition of the CO_2-rich solvent streams. In particular, the CO_2 loading of the rich solvent exiting the absorption column (stream 17 in Figure 3) is monitored to ensure it remains below the upper solid-phase solubility limit, assumed to be 0.80 mol-CO_2/mol-PZ (corresponding to 0.40 mol-CO_2/mol-alkalinity), consistent with Figure 4 and what was reported by Cousins et al.[22]

The absorber packing heights (H_{ABS}) considered in the simulations are 8, 10, 12, 16, 20, and 22 m for 8 m PZ and 5 m PZ.

Figure 5 presents the trend of the Thermal Energy Requirement (TER), defined as the ratio between the duty at the reboiler of the regenerator and the amount of CO_2 removed in the absorber as a function of the lean loading at various absorber heights. Since the amount of CO_2 removed is constant (90%), the trends observed for the reboiler duty and TER are equivalent. The heat duty of the reboiler can be decomposed into three main contributions, (i) the energy required to drive the endothermic desorption reactions, (ii) the sensible heat needed to raise the solvent temperature to the reboiler operating conditions and (iii) the energy necessary to generate the stripping vapor that rises through the regeneration column for a given packing height.

In the case of 8 m PZ, each packing height exhibits the characteristic minimum-shaped trend. At low lean loadings, the dominant contribution to the TER arises from the generation of stripping vapor in the reboiler (iii), since lower lean loading targets require higher stripping vapor flow rates and, consequently, higher energy input. Conversely, at high lean loadings, the solvent flow rate increases, and the dominant contribution becomes the energy required to heat the solvent (ii). The minimum point of each curve therefore represents the optimal lean loading for the corresponding absorber height. To

https://doi.org/10.1021/acs.energyfuels.5c05996
Energy Fuels 2026, 40, 6901−6918

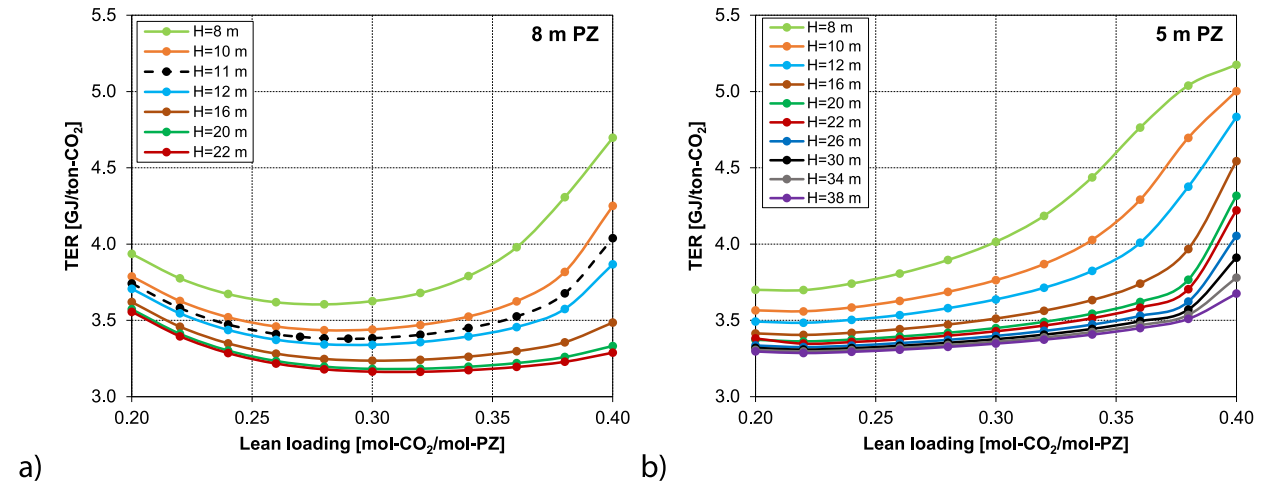

Figure 5. TER [GJ/ton-CO_2] as a function of the lean loading [mol-CO_2/mol-PZ] at various H_{ABS} [m] for a) 8 m PZ solution and b) 5 m PZ solution.

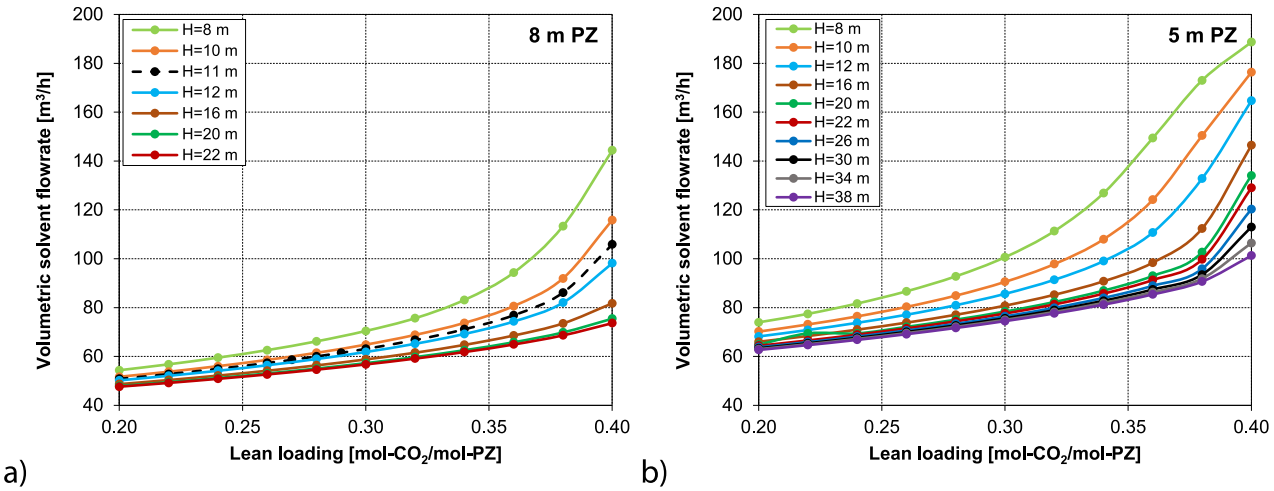

Figure 6. Volumetric solvent flow rate [m^3/h] as a function of the lean loading [mol-CO_2/mol-PZ] at various H_{ABS} [m] for a) 8 m PZ solution and b) 5 m PZ solution.

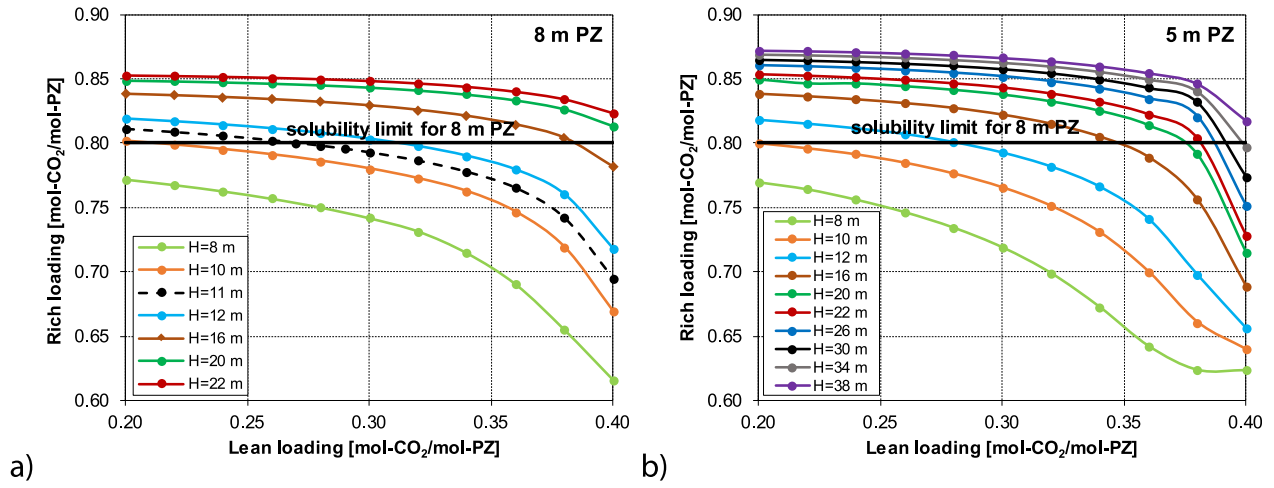

Figure 7. Rich loading [mol-CO_2/mol-PZ] as a function of the lean loading [mol-CO_2/mol-PZ] at various H_{ABS} [m] for a) 8 m PZ solution and b) 5 m PZ solution. A solubility limit corresponding to a loading of 0.8 mol-CO_2/mol-PZ is considered, selected as a slightly lower value than the solubility limit at 0 °C for an 8 m PZ solution (to be conservative), and superimposed on the graphs.

determine the most suitable combination of lean loading and H_{ABS}, several considerations must be made. As shown in Figure 5a, for a given lean loading, higher packing heights lead to lower TER. This occurs because, at constant lean loading, a taller absorber requires a lower solvent flow rate to achieve the 90% CO_2 removal target (Figure 6a), thereby reducing the TER and

https://doi.org/10.1021/acs.energyfuels.5c05996
Energy Fuels 2026, 40, 6901−6918

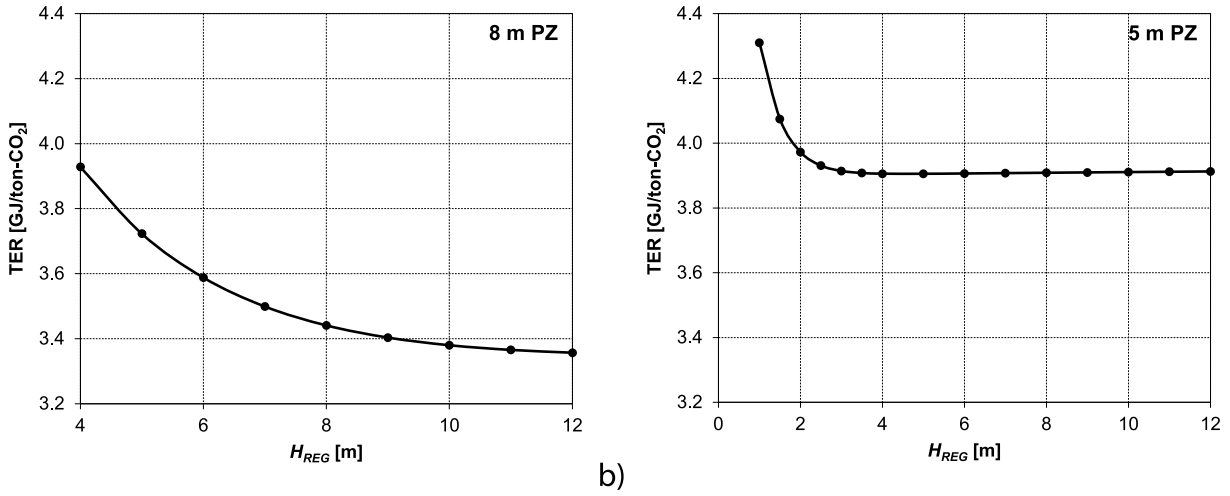

Figure 8. TER [GJ/ton-CO_2] as a function of the H_{REG} [m] for a) 8 m PZ solution and b) 5 m PZ solution.

operating costs. However, increasing the absorber height leads to higher investment costs, which must also be taken into account.

Nonetheless, these economic considerations alone are insufficient to determine the optimal values of the two parameters, as the behavior of the rich loading within the sensitivity analysis must also be taken into account (Figure 7a).

As shown in Figure 7a, at a constant H_{ABS}, increasing the lean loading decreases the rich loading because a larger solvent flow rate is required (see Figure 6a). Conversely, at a constant lean loading, the rich loading increases with H_{ABS} owing to the lower solvent flow rate used (see Figure 6a). Given that the upper solid-phase solubility limit is assumed to be 0.80 mol-CO_2/mol-PZ, in the case of 8 m PZ packing heights of 16, 20, and 22 m are unsuitable for the entire, or nearly the entire, range of lean loadings considered. For a packing height of 12 m and a corresponding optimal lean loading of 0.30 mol-CO_2/mol-PZ, the constraint is not satisfied for stream 17 (rich loading = 0.803 mol-CO_2/mol-PZ). In contrast, the constraint is met for shorter columns, though at the expense of higher TER and, thus, higher operating costs. The choice of the optimal H_{ABS} must also consider that given the rising cost of energy, accepting a higher capital cost for a taller column may be advantageous if it leads to lower energy consumption. To explore this trade-off, an additional simulation is performed with H_{ABS} = 11 m to identify a minimum lean loading associated with a reasonably low TER while still satisfying the solid solubility constraint for the rich loading. For this configuration, the optimal lean loading of 0.28 mol-CO_2/mol-PZ satisfies the constraint (rich loading = 0.793 mol-CO_2/mol-PZ). A refined analysis around the minimum identified a slightly higher lean loading of 0.29 mol-CO_2/mol-PZ as yielding the lowest reboiler duty, with the solid solubility limit still being respected (rich loading of 0.796 mol-CO_2/mol-PZ). Based on these findings, a H_{ABS} of 11 m is selected as the optimal configuration. Accordingly, in the subsequent analyses for 8 m PZ, a H_{ABS} of 11 m and a lean loading of 0.29 mol-CO_2/mol-PZ are adopted.

In the case of 5 m PZ, the effect of the H_{ABS} on the TER, volumetric solvent flow rate, and rich loading is exactly the same as the one observed for the 8 m PZ case (Figures 5b–7b). Similarly, the influence of the lean loading on the rich loading follows the same trend already identified for 8 m PZ (Figure 7b). However, with regard to the effect of the lean loading on the TER, as shown in Figure 5b, a slight minimum is observed at a lean loading of 0.22 mol-CO_2/mol-PZ for each packing height. The trend differs significantly from that obtained for 8 m PZ in Figure 5a. In fact, for 5 m PZ, the minimum is not very pronounced, and the TER increases almost monotonically with lean loading over the analyzed range. This behavior is likely due to the fact that, for 5 m PZ, the solvent flow rate required at the same H_{ABS} and lean loading is substantially higher than for 8 m PZ (Figure 6), since the solution is more diluted. This effect dominates across nearly the entire lean loading range studied, recalling that the solvent flow rate increases with lean loading. It can also be observed that for 5 m PZ, the solvent flow rate increases more rapidly with the CO_2 loading in the lean solvent stream compared to 8 m PZ. Despite the presence of a slight minimum in TER at 0.22 mol-CO_2/mol-PZ, this value lies very close to the lower solubility limit at 35–40 °C (Figure 4). Moreover, the reduction in the TER at this minimum is too small to justify selecting such a low lean loading as the optimal value. For these reasons, the optimal lean loading is chosen based on the value reported by Closmann et al.,[23] where a lean loading of 0.40 mol-CO_2/mol-PZ is used for 5 m PZ in order to remain sufficiently distant from the lower solubility limit. Theoretically, as can be observed in Figure 4, for 5 m PZ, unlike 8 m PZ, no upper solubility limit exists, and it would therefore be possible to operate at a rich loading higher than 0.80 mol-CO_2/mol-PZ. Nevertheless, in this analysis, and in analogy with the 8 m PZ case, a limit of 0.80 mol-CO_2/mol-PZ is imposed on the CO_2 content of the rich solvent exiting the absorber. Furthermore, no evidence is found in the literature of operation beyond this value. Recalling the influence of H_{ABS} on TER, and aiming to minimize the TER, the study range for H_{ABS} is extended to include packing heights of 26, 30, 34, and 38 m. As shown in Figure 7b, for a packing height of 34 m and a lean loading of 0.40 mol-CO_2/mol-PZ, the rich loading (0.797 mol-CO_2/mol-PZ) is only slightly below the imposed upper limit. This is not a major concern, since several studies report operation up to 0.80 mol-CO_2/mol-PZ.[23,29] However, it can be observed that, for this lean loading, the increase in TER when decreasing H_{ABS} from 34 m to 30 m is not particularly large (about 0.13 GJ/ton-CO_2 out of a total of around 3.8 GJ/ton-CO_2). Moreover, a lower packing height reduces the investment cost. For these reasons, a packing height of 30 m is selected as the optimal H_{ABS} in the case of 5 m PZ.

https://doi.org/10.1021/acs.energyfuels.5c05996
Energy Fuels 2026, 40, 6901–6918

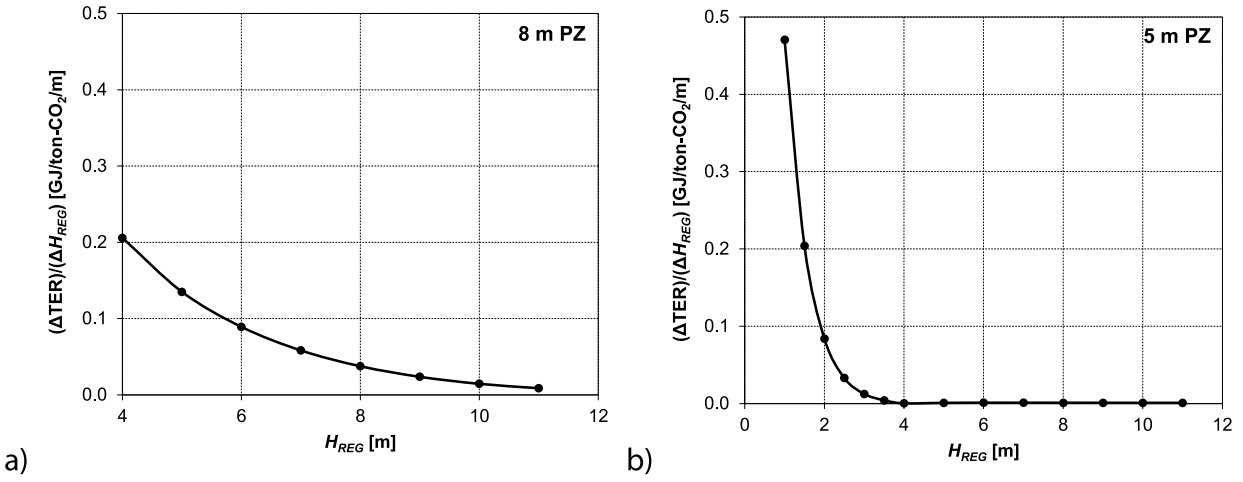

Figure 9. $\Delta TER/\Delta H_{REG}$ [GJ/ton-CO_2/m] as a function of the H_{REG} [m] for a) 8 m PZ solution and b) 5 m PZ solution.

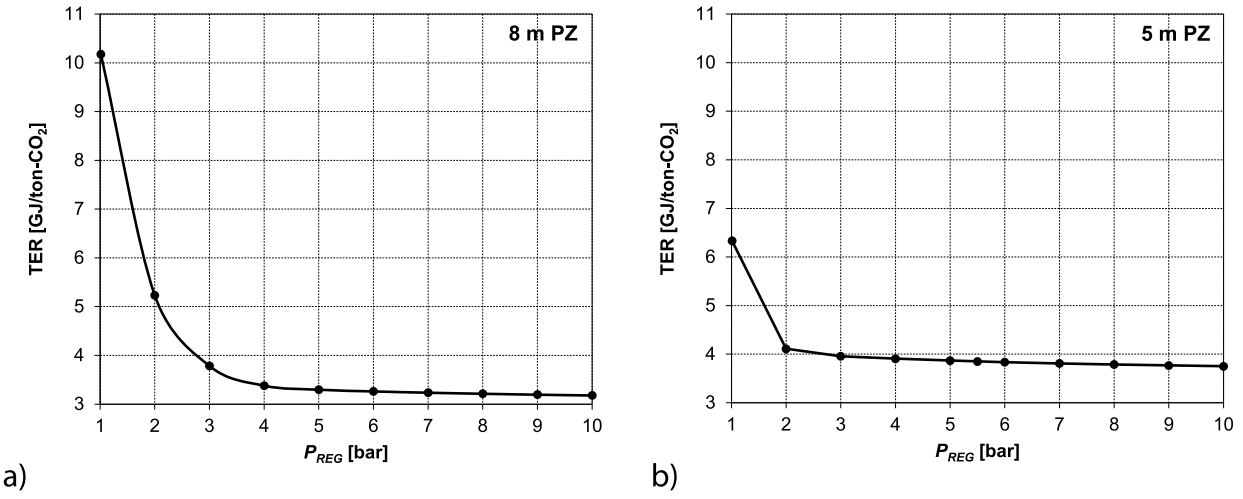

Figure 10. TER [GJ/ton-CO_2] as a function of the P_{REG} [bar] for a) 8 m PZ solution and b) 5 m PZ solution.

5.1.2. Choice of the Regenerator Packing Height. Using the optimal values of lean loading and H_{ABS} previously determined, a further sensitivity analysis is carried out on the regenerator packing height (H_{REG}). The H_{REG} is varied between 4 m and 12 m in increments of 1 m, and the effect of this parameter on TER is analyzed. Specifically, the analysis begins at a H_{REG} of 4 m, which is progressively increased until a plateau is observed in the TER trend.

In these simulations, the absorption, washing and pretreatment sections are kept unchanged. Therefore, the results related to these process sections (such as rich loading and solvent flow rate) remain the same as those obtained with the optimal H_{ABS} and lean loading for each H_{REG} value. Consequently, the constraint on the rich loading remains satisfied, regardless of the optimal regenerator packing height identified.

As shown in Figure 8, increasing the height of the regeneration column results in a decrease in TER and hence in operating costs, but entails greater capital investment.

When selecting the optimal H_{REG}, the recent significant rise in energy prices is also taken into consideration,[50] as in the previous analysis. The observed decrease in TER becomes progressively less pronounced at higher packing heights, which is a key factor in determining the optimal configuration. To this purpose, the incremental ratio (forward finite difference) between the thermal energy requirement and the regenerator packing height is also analyzed. Figure 9 shows this ratio as a function of the H_{REG}.

In the case of 8 m PZ, from the trend observed in Figure 9a, it can be seen that beyond a packing height of approximately 9−10 m, the reduction in TER becomes negligible (less than 1% per 1 m increment), despite the corresponding increase in H_{REG} and, thus, in capital costs. Therefore, in this case, the initially assumed value of H_{REG} = 10 m is confirmed as the optimal regenerator packing height.

In the case of 5 m PZ, since the TER trend within the range 4−12 m is found to remain essentially flat (Figure 9b), the study is extended to include packing heights down to 1 m, using a step size of 0.5 m between 4 and 1 m. As shown in Figure 9b, the TER value remains nearly constant for H_{REG} values above approximately 3 m. Since such a small packing height would be unrealistic for an industrial-scale column, a higher value is selected as the optimal H_{REG}. Specifically, a height of 7 m is chosen, in line with the configurations adopted in existing plants reported by Closmann et al.[23] and Cousins et al.[22]

5.1.3. Choice of the Regeneration Column Pressure. After determining the optimal packing height for the regenerator, an analysis is carried out to assess the influence of the column operating pressure (P_{REG}) on the TER. The pressure range examined extends from 1 to 10 bar, with increments of 1 bar. As in the analysis related to H_{REG}, the absorption, washing

https://doi.org/10.1021/acs.energyfuels.5c05996
Energy Fuels 2026, 40, 6901−6918

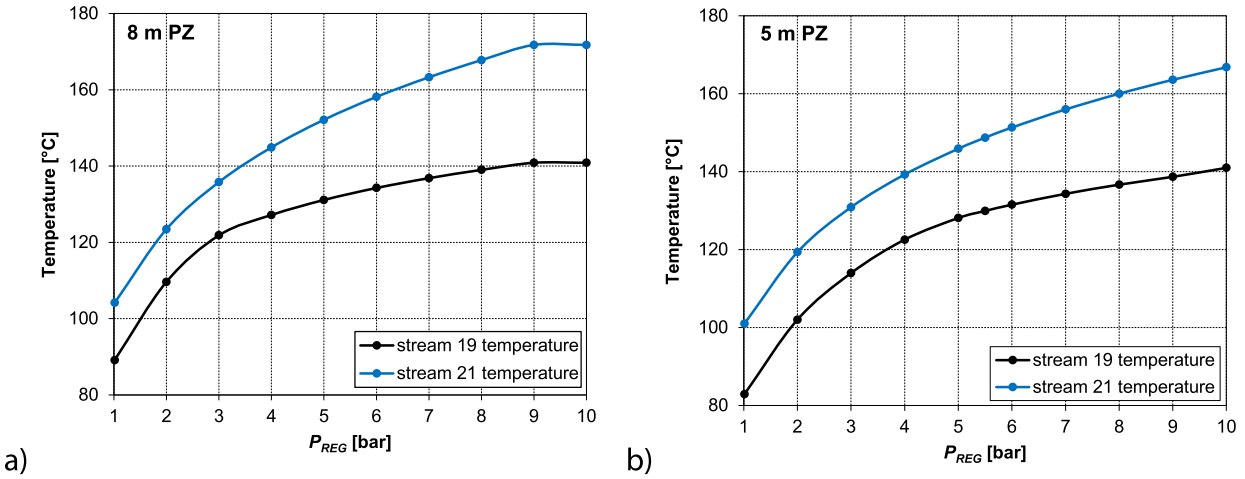

Figure 11. Temperature of the rich solvent entering the regenerator (stream 19) [°C] and temperature of the lean solvent exiting the regenerator (stream 21) as a function of the P_{REG} [bar] for a) 8 m PZ solution and b) 5 m PZ solution.

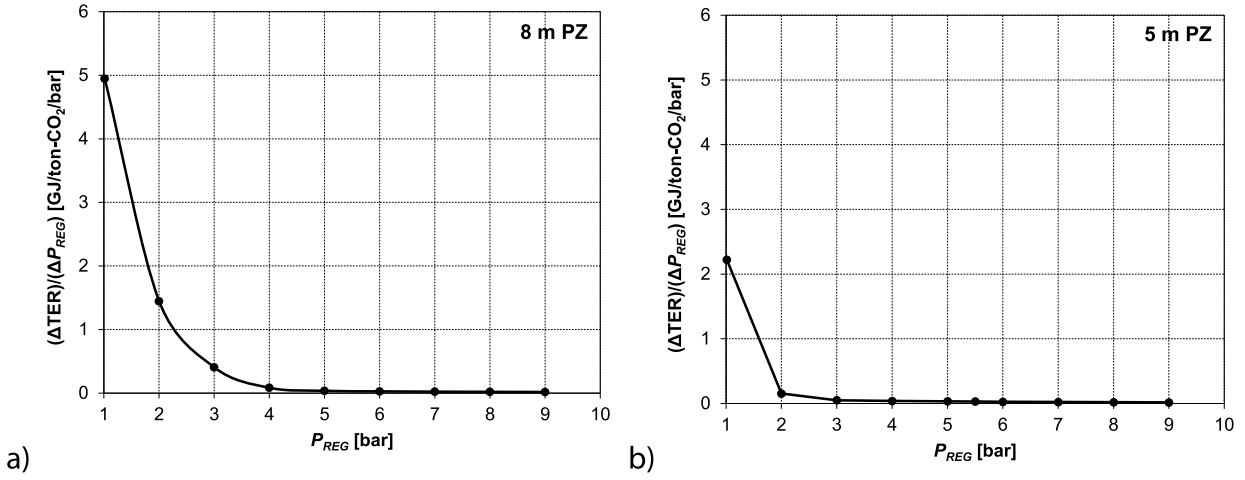

Figure 12. $\Delta TER/\Delta P_{REG}$ [GJ/ton-CO_2/bar] as a function of the P_{REG} [bar] for a) 8 m PZ solution and b) 5 m PZ solution.

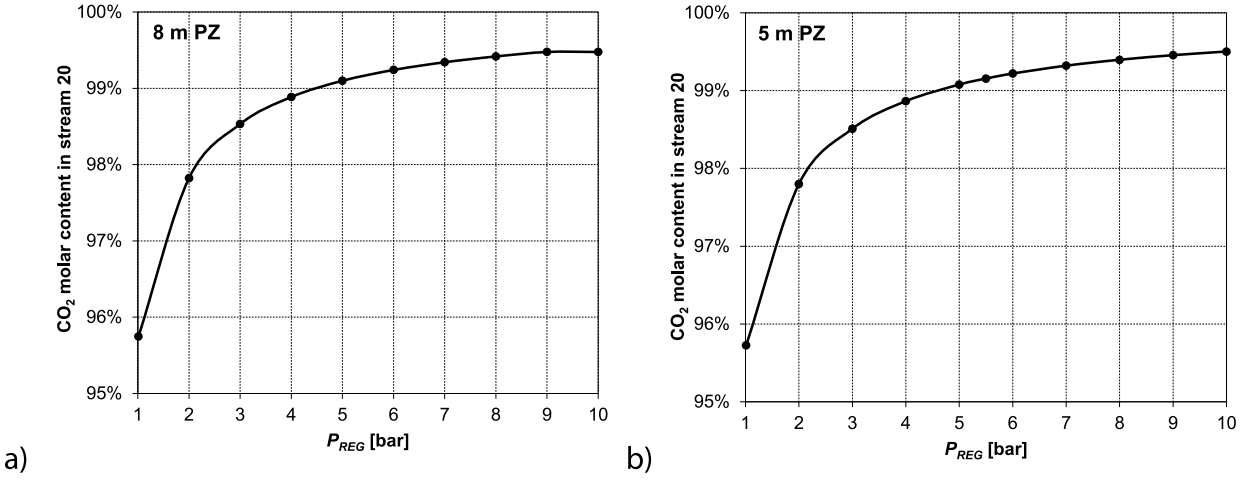

Figure 13. CO_2 molar content in the CO_2 product stream (stream 20) [%] as a function of the P_{REG} [bar] for a) 8 m PZ solution and b) 5 m PZ solution.

and pretreatment sections are not modified in these simulations. As shown in Figure 10, increasing the regenerator pressure leads to a progressive decrease in the TER until a plateau is reached.

This trend can be explained by the fact that a higher column pressure increases the temperature of the bottom product (stream 21 in Figure 3), as illustrated in Figure 11. Consequently, this stream transfers a greater amount of thermal energy to the rich solvent (stream 18 in Figure 3) within the lean-rich heat exchanger (LRHX in Figure 3), thereby increasing the temperature of the rich solvent entering the regenerator

https://doi.org/10.1021/acs.energyfuels.5c05996
Energy Fuels 2026, 40, 6901−6918

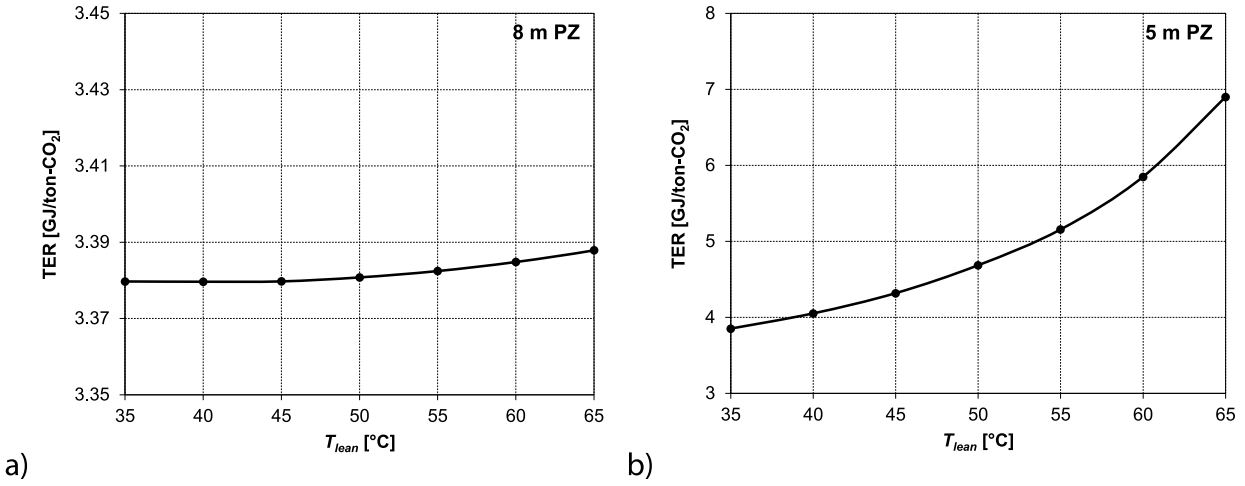

Figure 14. TER [GJ/ton-CO_2] as a function of the T_{lean} [°C] for a) 8 m PZ solution and b) 5 m PZ solution.

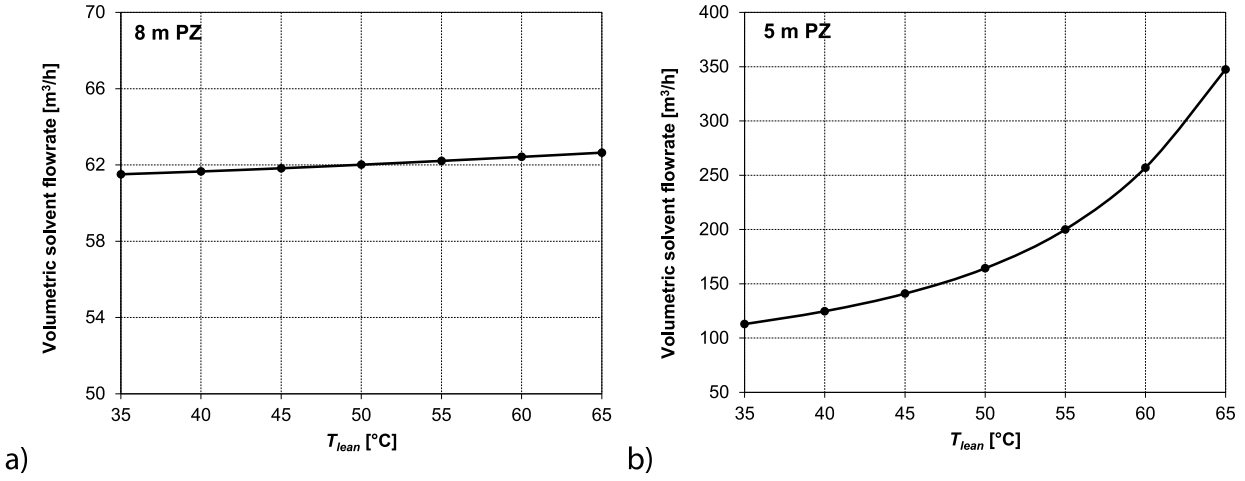

Figure 15. Volumetric solvent flow rate [m^3/h] as a function of the T_{lean} [°C] for a) 8 m PZ solution and b) 5 m PZ solution.

(stream 19 in Figure 3) (Figure 11). With a higher enthalpy content in stream 19, the thermal power required at the reboiler decreases.

The pressure beyond which further increases yield negligible improvements in TER is approximately 4 bar for both 8 m PZ and 5 m PZ (Figure 12). As shown in Figure 11, the temperature increase of stream 19 becomes less significant beyond this value, and the same trend is observed for stream 21.

Another contributing factor to the decrease in TER with increasing P_{REG} that results in a decrease in TER is the shift in vapor−liquid equilibrium within the column, which results in a higher molar fraction of CO_2 in the vapor phase (Figure 13).

In principle, operating the regenerator at higher pressures entails greater pumping costs to raise the outlet stream from the absorber (which operates near atmospheric pressure) to the regenerator pressure. However, in this case, the associated increase in pumping power is negligible. It should also be noted that operating the regenerator at higher pressures requires constructing a column with thicker walls, resulting in higher investment costs but also with a smaller diameter, which partially offsets the increased expense. An additional benefit of higher regenerator pressure, not explicitly accounted for in the present analysis, is the lower power demand of the downstream CO_2 compression. To fully assess the combined impact of these two opposing factors and, thus, of pressure on the investment cost, an economic analysis varying P_{REG} would be necessary.

Another important consideration when selecting the optimal regenerator pressure is that a higher pressure results in a higher column bottom temperature (corresponding to the temperature of stream 21, as shown in Figure 11). Although piperazine exhibits greater thermal stability than MEA, a reasonable upper limit for the bottom temperature is around 150 °C.[20,51,52] The rationale for selecting this value is discussed in detail by Babu and Rochelle.[53] In summary, if the temperature is too low, the column operates at a lower pressure, leading to a larger column diameter and a higher reboiler duty; conversely, if it is too high, excessive solvent degradation may occur. Therefore, a temperature of 150 °C appears to represent a good compromise.

To determine the optimal P_{REG}, the trend shown in Figure 12 is again determining. In the case of 8 m PZ, the decrease in TER with increasing P_{REG} becomes very small beyond a pressure of 4 bar (less than 3% per increment). Moreover, at this pressure, the column operates close to the desired bottom temperature of 150 °C, specifically around 145 °C, as shown in Figure 11a. This temperature will not change significantly in subsequent sensitivity analyses. Therefore, since higher P_{REG} would theoretically increase pumping costs, yield only marginal reductions in TER, and may exceed the recommended bottom temperature (Figure 11a), the regenerator operating pressure is

https://doi.org/10.1021/acs.energyfuels.5c05996
Energy Fuels 2026, 40, 6901−6918

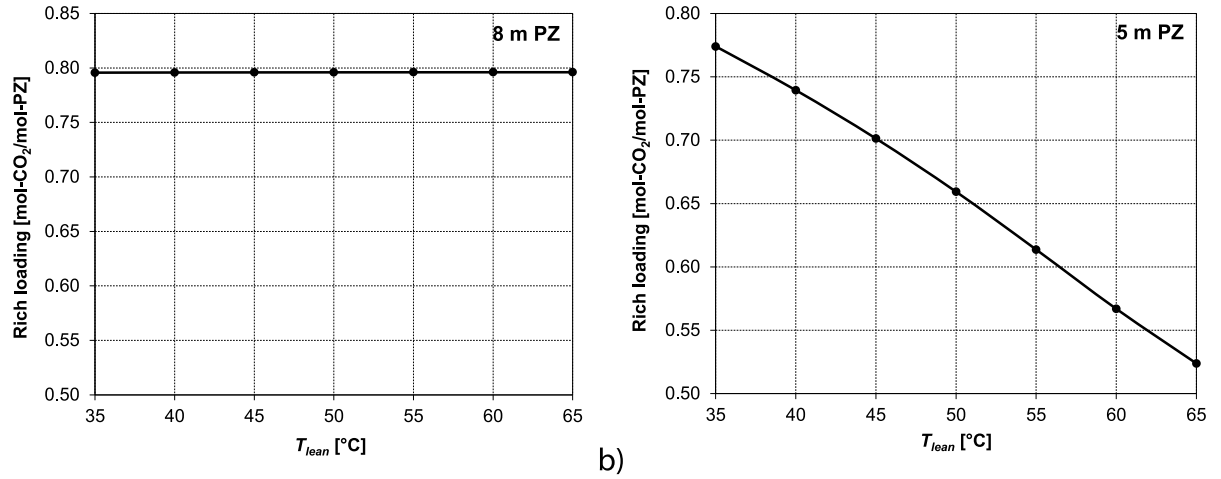

Figure 16. Rich loading [mol-CO_2/mol-PZ] as a function of the T_{lean} [°C] for a) 8 m PZ solution and b) 5 m PZ solution.

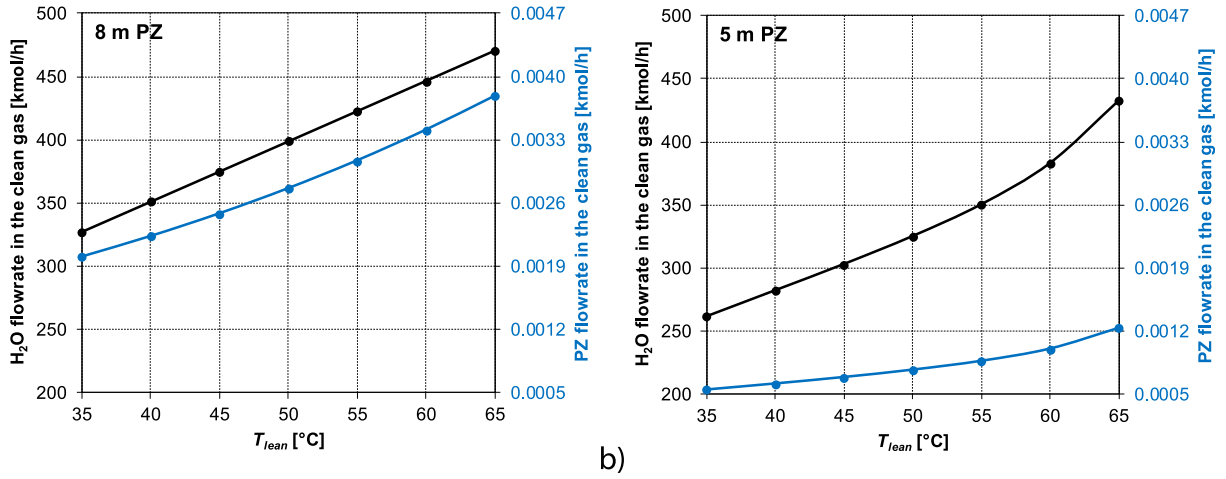

Figure 17. H_2O and PZ flow rates in the clean gas [kmol/h] as a function of the T_{lean} [°C] for a) 8 m PZ solution, and b) 5 m PZ solution.

set to 4 bar. In the case of 5 m PZ, increasing P_{REG} above 3−4 bar does not provide any significant benefit in terms of TER. An optimal pressure of 5.5 bar is selected in this case, in agreement with the findings reported by Babu and Rochelle.[53] Moreover, this pressure corresponds to a column bottom temperature close to 150 °C (148.7 °C, Figure 11b).

5.1.4. Choice of the Lean Solvent Temperature. This sensitivity analysis examines the temperature of the lean solvent (T_{lean}) entering the absorber (stream 16 in Figure 3). The temperature is varied between 35 and 65 °C, with increments of 5 °C. A temperature of 62 °C is the highest lean solvent temperature reported in the literature.[23] The lower bound of 35 °C is typical for amine absorption processes used in natural gas purification,[54] and, in general, the solvent temperature is maintained approximately 5 °C above the gas temperature to prevent further water condensation.

In the case of 8 m PZ, a very slight minimum in the TER trend is observed at around 40 °C, as shown in Figure 14a. However, since the difference relative to the value calculated at 35 °C is minimal (approximately 0.02%), this minimum is likely due to the limited numerical accuracy of the simulator. Overall, for both 8 m and 5 m PZ, the TER increases with rising T_{lean}. This behavior can be attributed to the fact that, as T_{lean} increases, a higher solvent flow rate is required to achieve the specified CO_2 removal (Figure 15), since CO_2 absorption is favored at lower temperatures. Consequently, a larger amount of solvent must be heated in the regenerator reboiler, leading to a higher TER. This increase is more pronounced for 5 m PZ than for 8 m PZ. At lower T_{lean} values, the TER trend approaches a plateau. For this reason, the analysis is not extended below 35 °C. Moreover, operating at lower temperatures would bring the system too close to the solid solubility limit (Figure 4), increasing the risk of precipitation.

The rich loading remains approximately constant as T_{lean} increases in the case of 8 m PZ (Figure 16a), since, despite the higher solvent flow rate, greater amounts of water and piperazine are lost in the clean gas stream (Figure 17a). Conversely, in the case of 5 m PZ, the rich loading decreases with increasing T_{lean} (Figure 16b) because the solvent flow rate rises much more rapidly than in the 8 m PZ case.

Considering that a lean solvent temperature of 40 °C is commonly reported in the literature,[28,29,49] this value is selected as the optimal operating condition for both 8 m PZ and 5 m PZ. Furthermore, operating at 40 °C, rather than 35 °C, provides an additional advantage by maintaining a greater margin from the solid solubility curve at equivalent CO_2 loadings.

5.1.5. Choice of the Approach Temperature Difference in the Lean/Rich Heat Exchanger. The last sensitivity analysis focuses on the approach temperature difference in the lean-rich heat exchanger (ΔT). In all simulations, this

https://doi.org/10.1021/acs.energyfuels.5c05996
Energy Fuels 2026, 40, 6901−6918

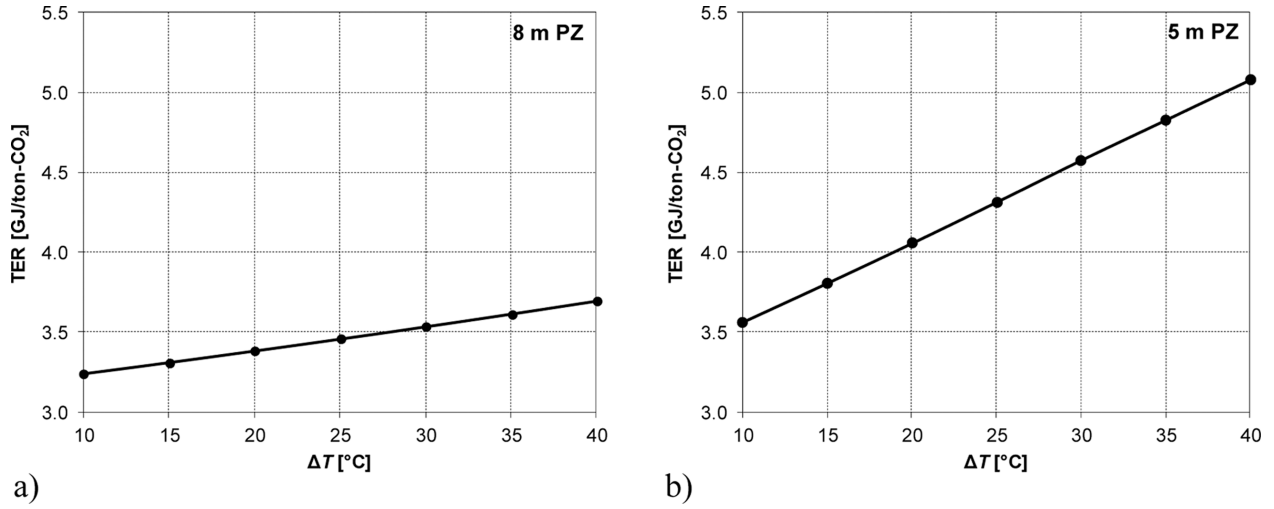

Figure 18. TER [GJ/ton-CO_2] as a function of the ΔT [°C] for a) 8 m PZ solution and b) 5 m PZ solution.

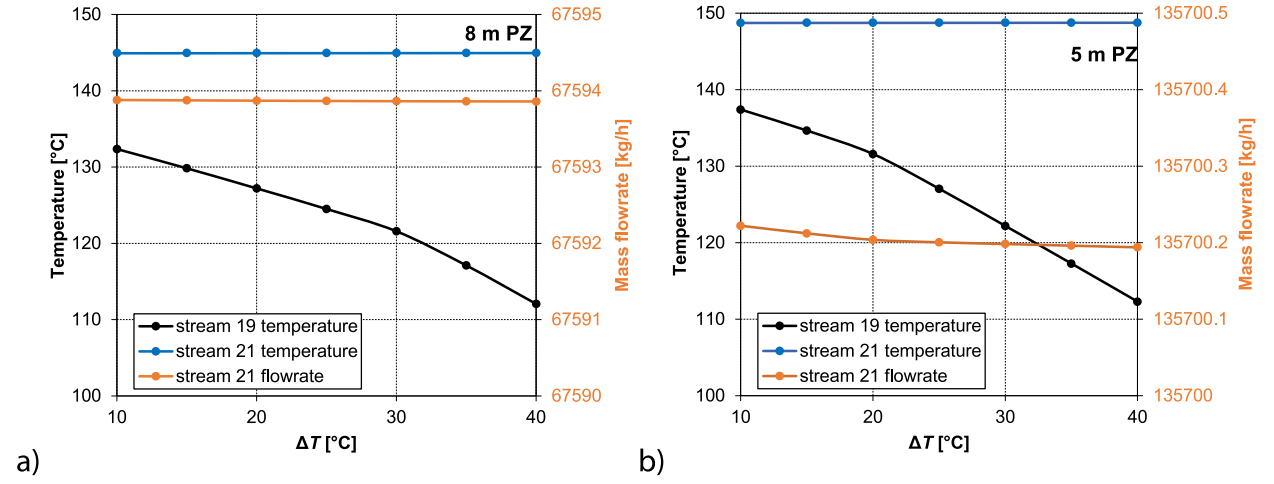

Figure 19. Temperature of the rich solvent entering the regenerator (stream 19) [°C], temperature of the lean solvent exiting the regenerator (stream 21) [°C] and mass flow rate of the lean solvent exiting the regenerator (stream 21) [kg/h] as a function of the ΔT [°C] for a) 8 m PZ solution and b) 5 m PZ solution.

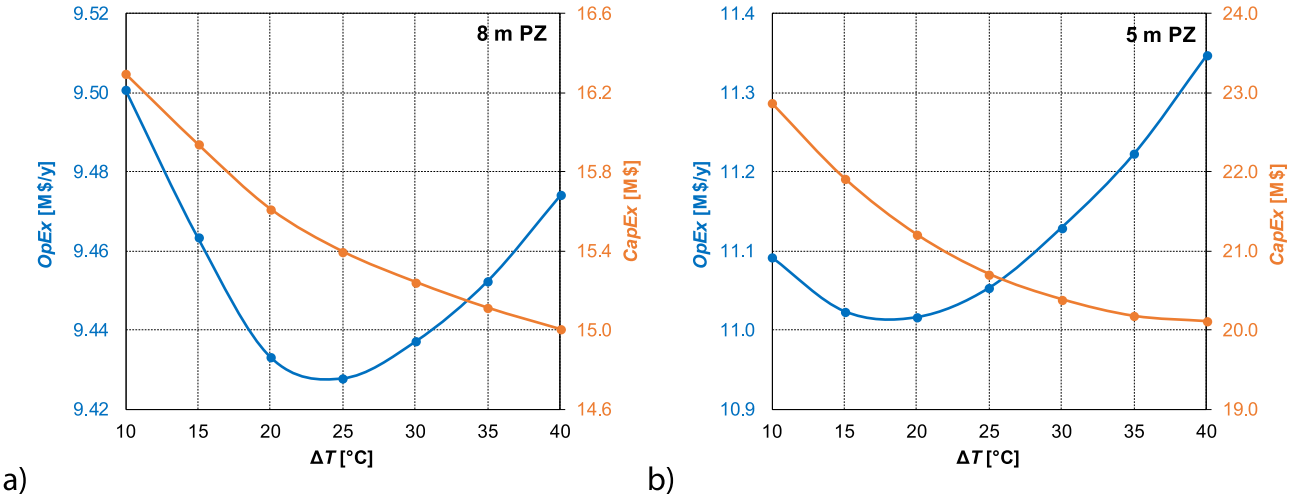

Figure 20. *OpEx* [M$/y] and *CapEx* [M$] as a function of the ΔT [°C] for: a) 8 m PZ solution and b) 5 m PZ solution.

temperature difference refers to the difference between the outlet temperature of the hot fluid (lean solvent) and the inlet temperature of the cold fluid (rich solvent). The analyzed range extends from 10 to 40 °C, with increments of 5 °C. As in the sensitivity analyses of H_{REG} and P_{REG}, the absorption section

https://doi.org/10.1021/acs.energyfuels.5c05996
Energy Fuels 2026, 40, 6901−6918

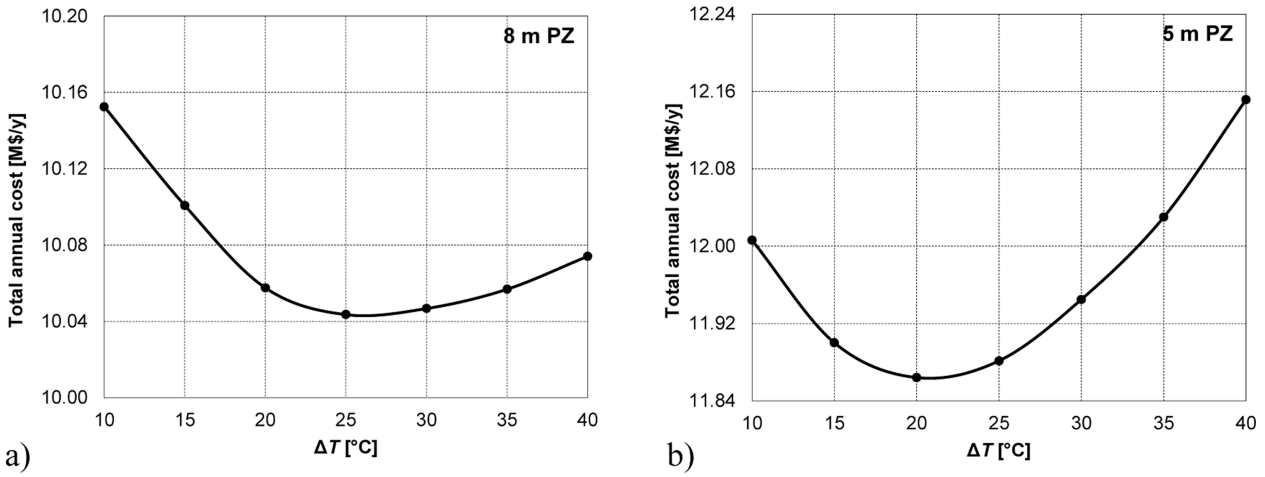

Figure 21. Total annual cost [M$/y] as a function of the ΔT [°C] for: a) 8 m PZ solution and b) 5 m PZ solution.

remains unchanged. Consequently, the results related to this part of the process are identical for each ΔT value.

As shown in Figure 18, increasing ΔT leads to an increase in the TER and consequently in the reboiler duty. This occurs because, while the temperature and flow rate of the lean solvent exiting the regenerator (stream 21) remain approximately constant across different ΔT values (Figure 19), a higher ΔT results in less heat being recovered in the lean-rich heat exchanger (LRHX in Figure 3). As a result, the temperature of the rich solvent entering the regenerator (stream 19) decreases (Figure 19).

On the other hand, a reduced heat recovery allows for a smaller heat exchanger, thereby lowering the process investment cost. To identify the optimal ΔT, the results of a preliminary economic analysis of the overall plant are determining. As shown in Figure 20, the *CapEx* decreases as ΔT increases, since one of its main contributions, the C_{BM} of LRHX, decreases with increasing ΔT. This is because the required heat transfer area becomes smaller as the exchanged heat decreases and the log-mean temperature difference (LMTD) across the exchanger increases. Conversely, the *OpEx* exhibits a minimum-shaped trend. Its main contribution arises from utility consumption, particularly the steam required to supply the thermal duty to the reboiler, that is proportional to the TER and thus increases with ΔT (Figure 18). However, for lower ΔT values, *OpEx* increases as ΔT decreases. This occurs because a lower ΔT leads to a higher *CapEx*, which in turn raises the operating cost components dependent on *CapEx*. This effect becomes especially relevant at low ΔT values when the increase in *CapEx* is more pronounced.

Analyzing the ΔT values in 5 °C increments reveals that the total annual cost reaches a minimum at 25 °C for the 8 m PZ case, as shown in Figure 21a. For the 5 m PZ case, the minimum temperature occurs at 20 °C, as shown in Figure 21b. It should be noted that this cost estimation is preliminary. Therefore, the plant cost values are not particularly significant, as several simplifying assumptions are made. The primary objective of this analysis is to highlight the order of magnitude of the total process costs and the influence of ΔT on both investment and operating costs.

The selection of these optimal values marks the conclusion of the optimization procedure.

5.2. Optimal Process

Based on the analyses performed, the features of the optimal process scheme for the designed CO_2 capture plant using aqueous PZ as a solvent applied to the flue gas of a waste-to-energy plant are reported in Table 5 for the different investigated PZ molal concentrations in the solvent.

Table 5. Values of the Design Variables for the Optimal Process Schemes of the 8 m and 5 m PZ Cases

	8 m PZ	5 m PZ
Lean loading [mol-CO_2/mol-PZ]	0.29	0.40
Absorber packing height, H_{ABS} [m]	11	30
Regenerator packing height, H_{REG} [m]	10	7
Regenerator operating pressure, P_{REG} [bar]	4	5.5
Lean solvent temperature, T_{lean} [°C]	40	40
Approach temperature difference in the lean-rich heat exchanger, ΔT [°C]	25	20

Considering the two optimal cases for 8 m and 5 m PZ, it is found that both the *CapEx* and the *OpEx* are higher in the latter case (Table 6). The main contributors to the investment cost are the absorption column, the lean-rich heat exchanger and the reboiler, with significantly higher values for the 5 m PZ case. The higher cost of the absorption column is due to its greater height and the higher costs of the lean-rich heat exchanger and the

Table 6. Optimal Process Performance for the 8 and 5 m PZ Cases

	8 m PZ	5 m PZ
Volumetric solvent flow rate [m^3/h]	61.65	124.8
Reboiler duty [kW]	6271	7357
TER [GJ/ton-CO_2]	3.454	4.052
Regenerator bottom temperature [°C]	145.0	148.7
Heat exchanged in the lean-rich heat exchanger [kW]	5009	10929
LMTD in the lean-rich heat exchanger [°C]	20.9	18.1
Mass flow rate of PZ in the absorber outlet gas [kg/h]	44.0484	12.9819
Mass flow rate of PZ in the clean gas [kg/h]	0.1923	0.0530
CapEx [M$]	15.39	21.21
OpEx [M$/y]	9.43	11.02
Total annual cost [M$/y]	10.04	11.86

https://doi.org/10.1021/acs.energyfuels.5c05996
Energy Fuels 2026, 40, 6901−6918

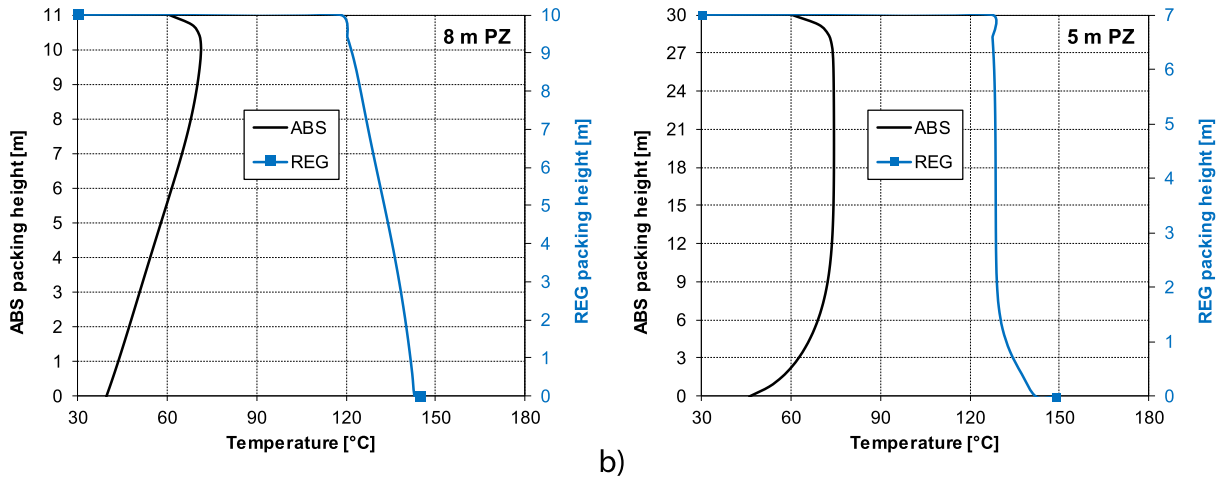

Figure 22. Temperature profile [°C] as a function of the packing height [m] in the absorption and regeneration columns for: a) 8 m PZ case and b) 5 m PZ case.

reboiler are primarily attributed to the larger thermal loads associated with these units in the 5 m PZ case (Table 6). This is mainly because a higher solvent flow rate is required, as the solution is less concentrated. The impact of this higher flow rate on costs also extends to other equipment, such as the pumps and compressor. Regarding the reboiler, since the regenerator operating pressure is slightly higher for 5 m PZ, the column bottom temperature is correspondingly higher (as illustrated by the temperature profiles in Figure 22). This results in a lower log-mean temperature difference in the reboiler, thus requiring a larger heat-transfer area. The main contributors to the operating cost are associated with utility consumption, which is lower in the 8 m PZ case due to reduced steam demand for providing the reboiler duty, as well as lower electricity consumption for driving the pumps because the flow rates involved are smaller. However, in the 8 m PZ case, the cost associated with raw materials is higher, since the required PZ makeup flow rate is greater. This occurs because the solution is more concentrated, and thus more PZ is lost in the clean gas stream (Table 6), considering that the washing water flow rate in the water-wash column is the same in both cases.

Therefore, according to the assumptions adopted in this study, the use of 8 m PZ appears to be economically more advantageous, by approximately 1.8 M$/y (around 15%). Nonetheless, as reported by Chen et al.,[28] from a practical standpoint, employing a 5 m PZ solution may be more beneficial, as the upper solid-phase solubility limit disappears. Moreover, as shown in Figure 4, the lower solid-phase solubility limit for 5 m PZ shifts to lower loading values at the same temperature. These factors, at least theoretically, provide a greater operational flexibility. Therefore, from the perspective of constructing an industrial plant, the use of a 5 m PZ solution may represent a more suitable choice for ensuring process flexibility. In practice, the actual operating temperatures during the lifetime of a plant may deviate significantly from those resulting from the process simulations. For instance, as reported by Cousins et al.,[22] during shutdown periods, the temperature in a pilot plant may drop to ambient levels, potentially causing amine precipitation. Moreover, seasonal variations may also lead to large temperature fluctuations, such as those arising from the wide thermal excursions between winter and summer. Consequently, some degree of solvent precipitation is generally unavoidable. However, in the case of 5 m PZ, this phenomenon is expected to be significantly mitigated.

6. CONCLUSIONS

In this work, a CO_2 capture plant using aqueous PZ as the solvent is designed for application to the flue gas of a waste-to-energy plant. The optimal design choices are determined through a series of sensitivity analyses on key process variables, namely lean loading, absorber packing height, regenerator packing height, regenerator operating pressure, lean solvent temperature and approach temperature difference in the lean-rich heat exchanger. From an economic standpoint, operating with a 8 m PZ solution is found to be more cost-effective than operating with 5 m PZ, in terms of both operating and investment costs. The total annual cost difference is approximately 1.8 M$/y (about 15%). This advantage mainly arises because the solvent flow rate required for 8 m PZ is significantly lower than that for 5 m PZ and, in addition, the investment cost associated with the absorption column is higher for the 5 m PZ case. However, since 5 m PZ exhibits a much wider solid-phase solubility range than 8 m PZ, from an industrial perspective, using a 5 m PZ solution could offer greater operational flexibility. Moreover, given the absence of an upper solubility limit for 5 m PZ, operation at a rich loading exceeding 0.80 mol-CO_2/mol-PZ may be feasible. This could be achieved, for instance, by increasing the absorber packing height at a constant lean loading, thus, reducing the thermal energy requirement for solvent regeneration. The conclusions drawn in this work are relative to PZ-based CO_2 capture from a reference waste-to-energy plant. However, they may be generalized and applied to other industrial contexts where the gas to be treated has a similar composition, particularly with respect to the CO_2 concentration.

AUTHOR INFORMATION

Corresponding Author

Stefania Moioli − *GASP - Group on Advanced Separation Processes & GAS Processing, Dipartimento di Chimica, Materiali e Ingegneria Chimica "G. Natta", Politecnico di Milano, Milano 20133, Italy;* orcid.org/0000-0002-7873-9193; Email: stefania.moioli@polimi.it

https://doi.org/10.1021/acs.energyfuels.5c05996
Energy Fuels 2026, 40, 6901−6918

Author

Federica Restelli − *GASP - Group on Advanced Separation Processes & GAS Processing, Dipartimento di Chimica, Materiali e Ingegneria Chimica "G. Natta", Politecnico di Milano, Milano 20133, Italy;* orcid.org/0009-0002-6142-2365

Complete contact information is available at: https://pubs.acs.org/10.1021/acs.energyfuels.5c05996

Author Contributions

The manuscript was written through contributions from all authors. All authors have given approval to the final version of the manuscript.

Notes

The authors declare no competing financial interest.

NOMENCLATURE

CapEx	capital expenditure
DEA	diethanolamine
LMTD	log-mean temperature difference
MEA	monoethanolamine
OpEx	operating expenditure
TEA	triethanolamine
PZ	piperazine
TER	thermal energy requirement

REFERENCES

(1) Spatolisano, E.; Pellegrini, L. A. Dehydration of IPA-H_2O mixture: Review of fundamentals and proposal of novel energy-efficient separation schemes. *Chem. Eng. Sci* **2023**, *273*, 118672.

(2) Minteer, S. D.11 - Biochemical production of other bioalcohols: Biomethanol, biopropanol, bioglycerol, and bioethylene glycol In *Handbook of Biofuels Production*. Luque, R.; Campelo, J.; Clark, J. Eds.; Woodhead Publishing: 2011. pp. 258−265.

(3) Ibrahim, H. Biofuel for sustainable (and eco-friendly) energy development. *Int. J. Eng. Comput. Sci* **2013**, *2*, 1584−1594.

(4) Singh, S.; Roy, S.; Prasad, L.; Chauhan, A. S.Bio-Alcohol: Production, Purification, and Analysis Using Analytical Techniques-*Biofuel Extraction Techniques*Wiley2023257−290

(5) Restelli, F.; Spatolisano, E.; Pellegrini, L. A. Energy and economic assessment of LH_2, NH_3, TOL/MCH and H0-DBT/H18-DBT for large-scale hydrogen transport. *Mater. Today Sustain.* **2025**, *31*, 101187.

(6) Pellegrini, L. A.; Spatolisano, E.; Restelli, F.; De Guido, G.; de Angelis, A. R.; Lainati, A. Green H_2. In *Transport through LH_2, NH_3 and LOHC: Opportunities and Challenges*. Springer Nature: Switzerland, Cham, 2024.

(7) Spatolisano, E.; Matichecchia, A.; Pellegrini, L. A.; de Angelis, A. R.; Cattaneo, S.; Roccaro, E. Toluene as effective LOHC: detailed techno-economic assessment to identify challenges and opportunities. *Comput.-Aided Chem. Eng.* **2023**, *52*, 3245−3250.

(8) He, T.; Pachfule, P.; Wu, H.; Xu, Q.; Chen, P. Hydrogen carriers. *Nat. Rev. Mater* **2016**, *1* (12), 16059.

(9) Restelli, F.; Spatolisano, E.; Pellegrini, L. A. Hydrogen Liquefaction: a Systematic Approach to Its Thermodynamic Modeling. *Chem. Eng. Trans* **2023**, *99*, 433−438.

(10) Xu, X.-L.; Liu, Y.-H.; Cui, H.-F.; Liu, J.; Guo, R.-T. A Review on CO_2 Capture Using Phase Change Amine Absorbents. *Energy Fuels* **2026**, *40* (2), 1020−1041.

(11) Yuan, R.; Jiang, K.; Wang, H.; Li, K. Advances in second-generation PZ/AMP amine technology through energy and exergy optimization. *Sep. Purif. Technol* **2026**, *380*, 135183.

(12) Garcia, S.; Weir, H.; Van der Spek, M.; Saleh, A.; Charalambous, C.; Sanchez-Fernandez, E.; Ros, J.; Skylogianni, E.; Garcia Moretz-Sohn Monteiro, J.; Wiechers, G.Process Integration of Advanced Amine-based Solvents in Power and Industrial Plants: A New Benchmark for Post-combustion Carbon Capture?*Proceedings of the 15th Greenhouse Gas Control Technologies Conference*Elsevier202115−18

(13) Feron, P. H. M.; Cousins, A.; Jiang, K.; Zhai, R.; Garcia, M. An update of the benchmark post-combustion CO_2-capture technology. *Fuel* **2020**, *273*, 117776.

(14) Moioli, S.; Restelli, F.; Pellegrini, L. A.; Carrara, A. Review on Experimental Plants for CO_2 Removal Based on Ammonia. *Energy Fuels* **2026**, *40* (6), 2827−2849.

(15) Restelli, F.; Moioli, S.; Pellegrini, L. A. Review on CCUS Sections Applied to Waste to Energy Plants. *Energies* **2026**, *19*, 855.

(16) Neerup, R.; Rasmussen, V. E.; Vinjarapu, S. H. B.; Larsen, A. H.; Shi, M.; Andersen, C.; Fuglsang, K.; Gram, L. K.; Nedenskov, J.; Kappel, J.; Blinksbjerg, P.; Jensen, S.; Karlsson, J. L.; Borgquist, S.; Jørsboe, J. K.; Villadsen, S. N. B.; Fosbøl, P. L. Solvent degradation and emissions from a CO_2 capture pilot at a waste-to-energy plant. *J. Environ. Chem. Eng* **2023**, *11* (6), 111411.

(17) Moioli, S.; De Guido, G.; Pellegrini, L. A.; Fasola, E.; Riva, E. R.; Alberti, D.; Carrara, A. Techno-economic assessment of the CO_2 value chain with CCUS applied to a waste-to-energy Italian plant. *Chem. Eng. Sci* **2024**, *287*, 119717.

(18) Moioli, S.; Pellegrini, L. A.; Redolfi Riva, E.; Alberti, D.; Carrara, A. Application of Intercooling to the CO_2 Removal Section of an Italian Waste-To-Energy Plant. *Ind. Eng. Chem. Res* **2025**, *64* (18), 9349−9372.

(19) Dugas, R.; Rochelle, G. Absorption and desorption rates of carbon dioxide with monoethanolamine and piperazine. *Energy Procedia* **2009**, *1*, 1163−1169.

(20) Rochelle, G.; Chen, E.; Freeman, S.; Van Wagener, D.; Xu, Q.; Voice, A. Aqueous piperazine as the new standard for CO_2 capture technology. *Chem. Eng. J* **2011**, *171* (3), 725−733.

(21) Freeman, S. A.; Dugas, R.; Van Wagener, D. H.; Nguyen, T.; Rochelle, G. T. Carbon dioxide capture with concentrated, aqueous piperazine. *Int. J. Greenhouse Gas Control* **2010**, *4* (2), 119−124.

(22) Cousins, A.; Huang, S.; Cottrell, A.; Feron, P. H. M.; Chen, E.; Rochelle, G. T. Pilot-scale parametric evaluation of concentrated piperazine for CO_2 capture at an Australian coal-fired power station. *Greenhouse Gases: Sci. Technol.* **2015**, *5* (1), 7−16.

(23) Closmann, F.; Rochelle, G.; Gao, T.; Suresh Babu, A.; Abreu, M.; Drewry, B.FEED for Piperazine with the Advanced Stripperr™ on NGCC at Denver City, Texas*Proceedings of the 15th Greenhouse Gas Control Technologies Conference*Elsevier202115−18

(24) Freeman, S. A.; Davis, J.; Rochelle, G. T. Degradation of aqueous piperazine in carbon dioxide capture. *Int. J. Greenhouse Gas Control* **2010**, *4* (5), 756−761.

(25) Freeman, S. A.; Rochelle, G. T. Thermal degradation of aqueous piperazine for CO_2 capture. 1. Effect of process conditions and comparison of thermal stability of CO_2 capture amines. *Ind. Eng. Chem. Res* **2012**, *51* (22), 7719−7725.

(26) Gao, F.; Liu, Y.; Zhai, B.; Shi, J.; Wu, J.; Li, L.; Lu, S.; Yu, Y.; Liu, M.; Jing, D. Intensified plant-scale post-combustion CO_2 capture based on piperazine-activated methyldiethanolamine solution via cascaded stationary and rotating packed beds. *J. Clean. Prod* **2025**, *504*, 145359.

(27) AspenTech. *Aspen Plus*. AspenTech: Burlington (MA), United States, 2022.

(28) Chen, E.; Zhang, Y.; Lin, Y.; Nielsenb, P.; Rochelle, G. Review of recent pilot plant activities with concentrated piperazine. *Energy Procedia* **2017**, *114*, 1110−1127.

(29) Lin, Y.-J.; Madan, T.; Rochelle, G. T. Regeneration with rich bypass of aqueous piperazine and monoethanolamine for CO_2 capture. *Ind. Eng. Chem. Res* **2014**, *53* (10), 4067−4074.

(30) Cousins, A.; Cottrell, A.; Lawson, A.; Huang, S.; Feron, P. H. M. Model verification and evaluation of the rich-split process modification at an Australian-based post combustion CO_2 capture pilot plant. *Greenhouse Gases:Sci. Technol.* **2012**, *2* (5), 329−345.

(31) Izzi, R. *Ottimizzazione e analisi economica di schemi di processo per l'assorbimento di CO_2 con un solvente a base di piperazina*. MSc Thesis, Politecnico di Milano, 2022.

(32) Chen, C.-C.; Britt, H. I.; Boston, J. F.; Evans, L. B. Local composition model for excess Gibbs energy of electrolyte systems. Part I: Single solvent, single completely dissociated electrolyte systems. *AIChE J* **1982**, *28* (4), 588−596.
(33) Chen, C. C.; Evans, L. B. A local composition model for the excess Gibbs energy of aqueous electrolyte systems. *AIChE J* **1986**, *32* (3), 444−454.
(34) Mock, B.; Evans, L. B.; Chen, C. C. Thermodynamic representation of phase equilibria of mixed-solvent electrolyte systems. *AIChE J* **1986**, *32* (10), 1655−1664.
(35) Gross, J.; Sadowski, G. Perturbed-chain SAFT: An equation of state based on a perturbation theory for chain molecules. *Ind. Eng. Chem. Res* **2001**, *40* (4), 1244−1260.
(36) Gross, J.; Sadowski, G. Application of perturbation theory to a hard-chain reference fluid: an equation of state for square-well chains. *Fluid Phase Equilib* **2000**, *168* (2), 183−199.
(37) Gross, J.; Sadowski, G. Modeling polymer systems using the perturbed-chain statistical associating fluid theory equation of state. *Ind. Eng. Chem. Res* **2002**, *41* (5), 1084−1093.
(38) Pinsent, B. R. W.; Pearson, L.; Roughton, F. J. W. The kinetics of combination of carbon dioxide with hydroxide ions. *Trans. Faraday Soc.* **1956**, *52*, 1512−1520.
(39) Bishnoi, S.; Rochelle, G. T. Absorption of carbon dioxide into aqueous piperazine: reaction kinetics, mass transfer and solubility. *Chem. Eng. Sci* **2000**, *55* (22), 5531−5543.
(40) Bishnoi, S.; Rochelle, G. T. Absorption of carbon dioxide in aqueous piperazine/methyldiethanolamine. *AIChE J* **2002**, *48* (12), 2788−2799.
(41) Bravo, J.; Rocha, J. A.; Fair, J. Mass transfer in gauze packings. *Hydrocarbon Process.* **1985**, *64* (1), 91−95.
(42) Taylor, R.; Krishna, R. *Multicomponent mass transfer*. John Wiley & Sons, 1993.
(43) Turton, R.; Bailie, R. C.; Whiting, W. B.; Shaeiwitz, J. A. *Analysis, synthesis and design of chemical processes*. 3rd ed.; Pearson Education: 2008.
(44) Christensen, P.; Dysert, L. *Cost estimate classification system. AACE International recommended practice No. 17R-97*. AACE: Morgantown, WV, 2011.
(45) Pharmacompass. 2025 https://www.pharmacompass.com/price/piperazine.
(46) Moioli, S.; Pellegrini, L. A.; Ho, M. T.; Wiley, D. E. A comparison between amino acid based solvent and traditional amine solvent processes for CO_2 removal. *Chem. Eng. Res. Des* **2019**, *146*, 509−517.
(47) U.S. Energy Information Administration. *U.S. Natural Gas Industrial Price*. 2025 https://www.eia.gov/dnav/ng/hist/n3035us3m.htm.
(48) U.S. Energy Information Administration. *Electric Power Monthly*. 2025 https://www.eia.gov/electricity/monthly/epm_table_grapher.php?t=epmt_5_3.
(49) Lin, Y.-J.; Rochelle, G. T. Optimization of advanced flash stripper for CO_2 capture using piperazine. *Energy Procedia* **2014**, *63*, 1504−1513.
(50) Trading Economics. *Italy Electricity Price*. 2026 https://tradingeconomics.com/italy/electricity-price.
(51) Van Wagener, D. H. *Stripper modeling for CO_2 removal using monoethanolamine and piperazine solvents*. PhD dissertation, The University of Texas at Austin, 2011.
(52) Freeman, S. A. *Thermal degradation and oxidation of aqueous piperazine for carbon dioxide capture*. PhD dissertation, The University of Texas at Austin, 2011.
(53) Babu, A. S.; Rochelle, G. T. Process design of the piperazine advanced stripper for a 460 MW NGCC. *Int. J. Greenhouse Gas Control* **2022**, *115*, 103631.
(54) Kohl, A. L.; Nielsen, R. *Gas purification*. Gulf Professional Publishing: Houston, TX, 1997.

https://doi.org/10.1021/acs.energyfuels.5c05996
Energy Fuels 2026, 40, 6901−6918